

UNIVERSITY OF BAYREUTH

MICROMETEOROLOGY GROUP

Bachelor Thesis in Geoecology

---

**A study on quantitative detection and  
atmospheric transport of microplastic  
in a wind tunnel**

---

**Author:**

Anna-Lena URBANEK  
(1401200)

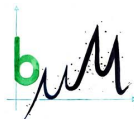
**Supervisor:**

Prof. Dr. Christoph THOMAS  
Micrometeorology

**Second reviewer:**

Prof. Dr. Martin OBST  
Experimental Biogeochemistry

March 6, 2019





# Abstract

Plastics are useful materials but over the past years, more and more studies showed the potential danger of the accumulation of microplastics in the environment. As the pathways, especially in the atmosphere, are poorly understood, this research examined the characteristics of atmospheric transport of microplastics and developed a method to detect microplastic particles quantitatively in a wind tunnel.

To do so, three different methods were tested utilizing fluorescent polyethylene spheres with a diameter of 53 - 63  $\mu\text{m}$ : fluorescence spectroscopy, fluorescence microscopy, and a photographic method comparing light intensities of glass slides with microplastic particles on before and after being exposed to the wind stream in the wind tunnel. All three methods were unsuccessful due to the low precision of the fluorescence spectroscopy, the low practicability of the microscope, and fluctuating light intensities between the two pictures with reasons other than particle movement. Hence, a new method was developed: a variation of the photographic method which was both practicable and precise. For this method, both photographs were overlaid so that the moved particles could be visualized and counted.

The applicability of this method was proofed in further experiments examining the characteristics of atmospheric transport of microplastic particles. After the characterization of the airflow in the wind tunnel including turbulence intensities and wind speeds at different settings of the tunnel, the tunnel was modified to enhance these parameters. The experiments on movement and suspension of microplastic particles into the airstream in the idealized environment of the wind tunnel were conducted by varying wind speed, experiment length and ionization. The results showed an increase in particle movement with increasing wind speeds. A decrease in the rate of erosion after the first minutes could not be observed. The critical friction velocity at given conditions was between 0.16 and 0.24  $\text{ms}^{-1}$ . First experiments varying ionization suggested that more factors might influence the erosion of microplastics, for example relative humidity.



# Zusammenfassung

Verschiedene Arten von Plastik sind zwar nützlich für unsere Gesellschaft, jedoch zeigten in vergangenen Jahren immer mehr Studien die potentiellen Gefahren der Akkumulation von Mikroplastik in der Umwelt. Da die Transportwege, vor allem in der Atmosphäre, noch schlecht verstanden sind, beleuchtete diese Studie die Eigenschaften des atmosphärischen Transports von Mikroplastik genauer und entwickelte eine Methode, um Mikroplastikpartikel in einem Windkanal quantitativ zu detektieren.

Dazu wurden drei verschiedene Methoden mit fluoreszierenden Polyethylensphären mit einem Durchmesser von 53 - 63  $\mu\text{m}$  getestet: Fluoreszenz-Spektroskopie, Fluoreszenz-Mikroskopie und eine photographische Methode, bei der Lichtintensitäten von Mikroplastikproben auf Glasträgern jeweils vor und nach einem Experiment verglichen wurden. Aufgrund der geringen Genauigkeit der Fluoreszenz-Spektroskopie, der geringen Praktikabilität des Mikroskops und fluktuierenden Lichtintensitäten der photographischen Methode, die nicht am Verlust von Partikeln lagen, wurde keine der drei Methoden verwendet, sondern es wurde eine einfache, doch trotzdem genaue Methode entwickelt: eine Variation der photographischen Methode, bei der die Photographien vor und nach dem Experiment exakt übereinander gelegt wurden, um so die bewegten Teilchen visualisieren und zählen zu können.

Die Anwendbarkeit dieser Methode wurde in weiteren Experimenten, die die Eigenschaften von atmosphärischem Transport von Mikroplastikpartikeln untersuchten, bestätigt. Nach der Charakterisierung des Luftstroms im Windtunnel, das Messung von Turbulenzintensitäten und Windgeschwindigkeiten bei verschiedenen Windtunneleinstellungen beinhaltete, wurde dieser modifiziert, um diese Parameter zu erhöhen. Für die Experimente, die zur Untersuchung von Bewegung und Suspension der Mikroplastikpartikeln dienten, wurden Windgeschwindigkeit, Experimentlänge und Ionisierung im Windkanal verändert. Mit ansteigender Windgeschwindigkeit konnte ein höherer Vertrag an Partikeln festgestellt werden. Ein Absinken der Erosionsrate nach den ersten Minuten des Experiments zeigte sich nicht. Die kritische Schubspannungsgeschwindigkeit zu gegebenen Bedingungen lag zwischen 0.16 und 0.24  $\text{ms}^{-1}$ . Erste Experimente zum Einfluss von Ionisation zeigten, dass mehr Faktoren einen Einfluss auf die Erosion von Mikroplastikpartikeln haben könnten, beispielsweise relative Luftfeuchtigkeit.



# Contents

<b>Abstract</b>	<b>i</b>
<b>Zusammenfassung</b>	<b>iii</b>
<b>Contents</b>	<b>iv</b>
<b>List of figures</b>	<b>vi</b>
<b>List of tables</b>	<b>viii</b>
<b>1 Introduction</b>	<b>1</b>
<b>2 Theory of wind erosion and particle transport</b>	<b>5</b>
2.1 Factors controlling wind erosion of small particles . . . . .	5
2.2 Processes of particle transport . . . . .	7
<b>3 Materials and Methods</b>	<b>13</b>
3.1 Microplastic particles . . . . .	13
3.2 The wind tunnel . . . . .	13
3.3 Methods to detect MP quantitatively . . . . .	21
3.3.1 Fluorescence Spectroscopy . . . . .	21
3.3.2 Fluorescence Microscopy . . . . .	23
3.3.3 Photographic method based on difference in light intensity	23
3.3.4 Visually counted MP with the photometric method . . .	25
3.4 Experiments on suspension of MP in the wind tunnel . . . . .	25
<b>4 Results and Discussion</b>	<b>27</b>
4.1 Results of the different methods . . . . .	27
4.1.1 Fluorescence Spectroscopy . . . . .	27
4.1.2 Fluorescence Microscopy . . . . .	30
4.1.3 Photographic method based on difference in light intensity	32
4.1.4 Photometric method . . . . .	33
4.1.5 Comparison of the different methods . . . . .	35
4.1.6 Recommendations to improve the methods and the ex- perimental setup . . . . .	36
4.2 Results of the experiments on MP suspension . . . . .	38

4.2.1	Impact of wind speed on MP suspension . . . . .	38
4.2.2	Impact of interparticle forces on MP suspension . . . . .	44
<b>5</b>	<b>Conclusion</b>	<b>47</b>
	<b>Acknowledgement</b>	<b>48</b>
	<b>Appendix</b>	<b>50</b>
	<b>Bibliography</b>	<b>52</b>
	<b>Declaration of Authorship</b>	<b>57</b>

# List of Figures

1.1	Schematic diagram of urban sources and potential pathways of macro- and microplastics with inputs in three environmental compartments: atmosphere, soil and water (Dris, 2016) . . . . .	2
2.1	Contour plot of wind tunnel deposition rate ( $\mu\text{gm}^{-2}\text{s}^{-1}$ ) around the cone (Parker et al., 2004) . . . . .	7
2.2	Different modes of particle transport: Creep, saltation and suspension (Shao, 2000) . . . . .	8
2.3	Conceptional model of crust erosion (Rice et al., 1999) . . . . .	9
2.4	Comparison of the Greeley-Iversen scheme and the simpler expression of Shao (Shao et al., 2000) . . . . .	12
3.1	Three polyethylene particles, covered with a green fluorescent film, with a size of 55, 57 and 62 $\mu\text{m}$ under the fluorescence microscope (Leica DM 5500 Q, Leica Microsystems, USA) . . . . .	14
3.2	Scheme of the wind tunnel with adjustment (modified from L. Pfister, pers. comm.) . . . . .	15
3.3	Wind tunnel mapping before adjustment at 0.2, 1.0 and 2.5 $\text{ms}^{-1}$	16
3.4	Photograph of the adjusted wind tunnel, taken from the back with view to the front . . . . .	16
3.5	Scheme of the test section in the wind tunnel with the mapping positions . . . . .	17
3.6	Logarithmic wind profiles at different mapping locations in the adjusted wind tunnel . . . . .	18
3.7	Logarithmic wind profiles for different fan speed settings . . . . .	19
3.8	Relation between friction velocity and mean wind speed at (2600,0,150), measured during the mapping of the adjusted wind tunnel at 2 min intervals (Fig. 3.7). . . . .	20
3.9	Wind speed values from experiment 13 to 32 (Table 4.2) at (2900,0,150) depending on the fan speed settings in the wind tunnel . . . . .	20
3.10	Workflow chart of the different methods tested . . . . .	22

3.11	Optical construction with camera, slide holder and slide with MP particles, placed in the Black Box. On the top, the UV lamp is installed. . . . .	24
4.1	Calibration lines of the fluorometer (LS-55, PerkinElmer, USA) for polyethylene spheres with a diameter of 53-63 $\mu\text{m}$ and concentrations of 50 to 5,000 particles per $\text{cm}^2$ . . . . .	28
4.2	Comparison of calculated and counted number of MP particles on the glass slide . . . . .	30
4.3	Relative deviation of the calculated number of MP particles on one glass slide from the counted number of MP particles using the microscope . . . . .	31
4.4	Comparison of two models plotted to the light intensity data of MP particle samples that were put in the Black Box and were excited by an UV lamp . . . . .	33
4.5	Close up of the construction for the photometric method . . . . .	34
4.6	Scheme of evaluation of the photometric method . . . . .	35
4.7	Comparison of particle movement related to wind speed at five different wind speeds (experiment 13 to 36) . . . . .	41
4.8	Comparison of particle movement over experiment length related to wind speed of five different wind tunnel configurations (a) and variation in ionization (b) (Table 4.2) . . . . .	42
4.9	Comparison of number of moved particles of experiments 29 to 32 (1st run without ionizer), 33 to 36 (2nd run without ionizer), 37 to 40 (1st run with ionizer), 41 to 44 (2nd run with ionizer) and 9 to 12 (experiment block A) at a wind speed of $6.3 \text{ ms}^{-1}$ with corresponding humidity values in the laboratory . . . . .	45

# List of Tables

3.1	Characteristics of the MP particles that were used in the experiments . . . . .	13
3.2	Overview of different experiments that were carried out in this research with the experiment parameters that were changed . .	26
4.1	Comparison of the MP particle concentration that can be measured, the preciseness and the practicability of the different methods that were tested . . . . .	35
4.2	Results of the experiments on MP suspension of this research . .	39



# 1. Introduction

As plastics have a wide range of use and a lot of positive characteristics, such as high plasticity, malleability, durability and low cost, there are millions of metric tons of plastics produced annually, the number still rising. In 2015, 322 million tons of plastics were produced globally whereas in 2016, the production rose up to 335 million tons (PlasticsEurope, 2018).

As a result, the deposition in the environment becomes more and more problematic. In 2016, 27.1 million tons of plastic waste were collected in Europe, including Norway and Switzerland, of which a third (31.1 %) was recycled whereas 41.6 % was used in energy recovery and the rest, 27.3 %, was deposited in landfills (PlasticsEurope, 2018). Through various pathways, the debris eventually accumulates in the soil or the ocean (Fig. 1.1). In 2010, estimated 4.8 to 12.7 million tons of plastics entered the ocean (Jambeck et al., 2015). This is only approximately 3 % of the global plastics production per year but the problem is the environmental accumulation.

By definition, a particle is called microplastic (MP) if its diameter is smaller than 5 mm. It can be further differentiated into large particles (1-5 mm) and small particles (1  $\mu\text{m}$  - 1 mm). MP particles, which were formed from a bigger plastic debris due to fragmentation are called secondary MP whereas primary MP is already produced in a small size to use them, for example, in cosmetics as skin cleaner products. The process of fragmentation can take place either mechanically or by being exposed to UV light for a longer time period. Biological degradation or disintegration are also causes for the degradation of a bigger plastic debris.

There are various sources of macro- and microplastics: landfill areas, traffic, industrial emission, urban infrastructure, sewage sludge, etc. (Dris, 2016). The debris can reach three environmental compartments: atmosphere, water, and soil (Fig. 1.1). The particles in the atmosphere will deposit as atmospheric fallout and may get into the freshwater through runoff and rainwater. Direct pollution by carelessly thrown away litter, for example, or debris from poorly managed landfill areas is also possible. Water treatment plants or combined sewer overflows are also sources for freshwater pollution. The remaining debris in the sewage sludge may contaminate the soils as well as through atmospheric fallout. Eventually, the debris either accumulates in the ocean or in the soil.

Especially the particles with a diameter of several  $\mu\text{m}$  are assessed to be

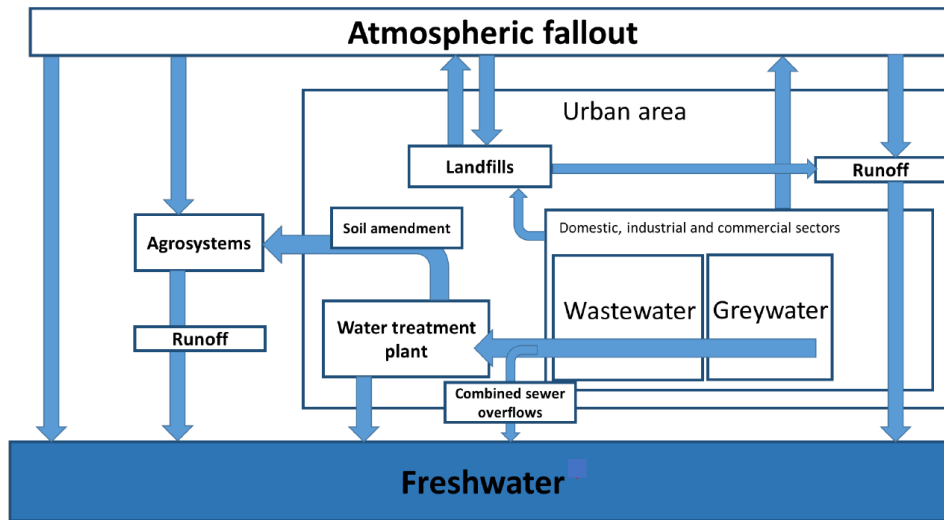


**Figure 1.1:** Schematic diagram of urban sources and potential pathways of macro- and microplastics with inputs in three environmental compartments: atmosphere, soil and water (Dris, 2016)

dangerous as they can be ingested by a wide range of organisms (Dris et al., 2015). The number of publications related to MP grew massively the last years. Recently, the existence of MP in human stool was verified in all samples of human stool from eight participants of which six ate sea food, two of them used chewing gum on a daily basis and all of them were in contact with plastic wrapped food during the observation period (Liebmann et al., 2018).

Microplastics seem to be ubiquitous as studies report contamination in various ecosystems:

- Marine water ecosystems  
Most of the publications concerning MP are related to MP particles in the marine environment. It was found in the oceans worldwide (Cole et al., 2011; Barnes et al., 2009), even in the arctic (Peeken et al., 2018).
- Freshwater ecosystems  
Studies on MP contamination in freshwater systems are largely focused on larger rivers and lakes for example lake Garda in Italy (Imhof et al., 2013) or lake Geneva in Switzerland (Alencastro, 2012). In Germany, Klein et al. (2015) studied samples from the river shores of the rivers Rhine and Main. Dris et al. (2015) pointed out after comparing recent studies on MP in freshwater ecosystems that the contamination is almost equal to that in marine ecosystems.

- Terrestrial ecosystem

Studies evaluating the MP concentration in soils are relatively rare even though MP can get into the soil either through the abrasion of plastic particles or through atmospheric deposition. Wastewater sludge is also a major source for synthetic fibers on fields (Zubris et al., 2005). In Nizzetto et al. (2016), a rough extrapolation of MP input on farmlands from data from Scandinavia was done. Some other studies (Lambert et al., 2014; Barnes et al., 2009; Rillig, 2012) mention the occurrence of MP in the terrestrial environment. MP particles not only impact the terrestrial ecosystem (Souza Machado et al., 2018) but also terrestrial organisms, for example earthworms (Huerta Lwanga et al., 2016).

- Atmosphere

A study of Dris et al. (2016) gave evidence for atmospheric MP. They compared samples of an urban and a sub-urban site where 2 to 355 particles $\text{m}^{-2}\text{day}^{-1}$  were found. The contamination in the urban site was higher. Half of the fibers were natural, the other half man made with 17 % purely synthetic fibers (Dris et al., 2016).

The atmosphere won't be a long term sink of MP particles because they will eventually settle out. However, it could be a very effective pathway for transporting the small debris over long distances. As the distribution of short-wave solar radiation over the world is different, the net energy at the surface is also different. More energy at the equator and less at the poles results in a pressure gradient. The wind that results from this pressure gradient and the Coriolis force, which acts on moving airstreams due to the rotation of the earth, is called geostrophic wind in the free atmosphere. Closer to the surface of the earth, in the atmospheric boundary layer, friction also influences the airstream besides pressure gradient and Coriolis force. So as a small particle gets entrained in the air, it can get into the free atmosphere and can get transported by the windstreams over a distance of hundreds to thousands of kilometers. Hence, it is important to get a better understanding of the suspension and transport mechanisms of MP particles. With the knowledge of the transport and fallout mechanisms of MP particles in the atmosphere, the atmospheric pollution can be reduced, which also has a positive effect on other ecosystems. The erosion of dust and sand has been more intensely studied and is better understood. However, mineral material of the same size fraction is different to MP concerning for example mass, density and electrical forces, this knowledge could serve as an analog for informing the MP specific research on the mechanisms of the atmospheric transport. While being able to only vary specific parameters, laboratory studies as a controlled environment can

be used to gain some fundamental understanding of the processes and forces of the erosion of MP particles.

This work aims to answer the following research questions:

- Which method is the most suitable to detect MP particles in a wind tunnel? Is a physical or a chemical approach better? How should the method look like, which construction is the best?
- What are the characteristics of atmospheric suspension and transport of MP particles in the wind tunnel?

To answer these questions, first, three methods of detecting MP were tested. Eventually, a fourth one was developed, which combines the advantages of the other methods. Subsequently, some experiments were carried out in the wind tunnel to test the method and to examine the characteristics of atmospheric transport of MP particles, i.a. the range of the critical friction velocity for the used MP particles. One expectation is to examine a positive correlation of particle movement with rising wind speed. For this, five different wind speeds were tested in the wind tunnel. The second expectation is to observe a decrease in the rate of erosion over time. To test this expectation, the experiments were conducted at four different experiment lengths. Varying the ionization in the tunnel should give information about the impact of electrical forces on the erosion of MP particles. The erosion is expected to be higher under usage of an ionizer as it should reduce the differences in electrical charge in the laboratory.

## 2. Theory of wind erosion and particle transport

Even though mineral particles differ from MP particles in various factors, i.e. form, mass, density and surface properties, the knowledge of wind erosion of dust and sand can be used for a first approach to the erosion of MP. Therefore, the important factors on wind erosion will be given here. The transport processes of small particles including relevant terminology such as creeping, saltation, and suspension will be defined in section 2.2.

### 2.1 Factors controlling wind erosion of small particles

As one of the main factors on wind erosion is the wind speed, the equation of the logarithmic wind profile is shown here (equation 2.1), which derived from considerations of Prandtl (1934). The wind speed  $U$  at a certain height  $z$  depends on the friction velocity  $u_*$ , the height  $z$  and the roughness length  $z_0$ .

$$U(z) = \frac{u_*}{\kappa} \ln \frac{z}{z_0} \quad (2.1)$$

Where:

- $U(z)$ : wind speed at height  $z$  ( $\text{ms}^{-1}$ )
- $u_*$ : friction velocity ( $\text{ms}^{-1}$ )
- $\kappa$ : Von Karman constant (1)
- $z$ : geometric height above surface (mm)
- $z_0$ : roughness length (mm)

The friction velocity  $u_*$  is a normalized momentum flux density. It is:  $u_* = (\tau\rho^{-1})^{0.5}$  with  $\tau$ , the surface drag, which itself is composed of the Reynolds shear stress and the viscous shear stress, and  $\rho$  as the air density. The Reynolds shear stress is important in the atmospheric boundary layer, above the viscous layer near the surface, where the momentum flux occurs mainly through turbulence. In this layer, the viscous shear stress is relative weak. In the viscous sublayer, they switch roles as the turbulence gets weak. Therefore, the Reynolds shear stress is small and the viscous shear stress gets

strong. Hence,  $\rho$  remains approximately constant with height in the atmospheric surface layer (Shao, 2000).

Another factor is the momentum roughness length, which describes the height at which the mean horizontal wind speed equals  $0 \text{ ms}^{-1}$  because of the high friction occurring near the surface. It describes the capacity of the surface for absorbing momentum (Shao, 2000) and depends on the surface roughness which is influenced in nature by non-erodible elements on the surface, such as vegetation or bigger soil fractions. As these elements reduce on the one hand the wind speed, hence shear force, and absorb on the other hand part of the momentum that is transferred from the atmosphere to the surface, they are one of the main control factors on wind erosion. A common measure for the vegetative cover is the frontal area index  $\lambda$ , which is dependent on the number of roughness elements on a specific ground area, including height and width of the elements. Shao et al. (1996) predicted the wind erosion to be zero when  $\lambda$  exceeds 0.15 at a friction velocity of  $0.43 \text{ ms}^{-1}$ .

Not only surface roughness has a great impact on wind erosion but also the particle roughness. Kim et al. (2016) included this factor in combination with surface properties and relative humidity in their research on resuspension rates.

Topography is another control factor on erosion and deposition. Parker et al. (2004) found out that an elevated topography has a huge effect on the pattern of deposition relative to a flat landscape (Fig. 2.1). They observed an increased deposition rate on the upwind face of a modelled elevation whereas in the wake, there was a larger area with a decreased deposition rate. The magnitude of the impact is dependent on the slope of the landscape. Experiments with a conical, three dimensional shape showed that there is not only more deposition on the windward face but also to the sides and the base of the shape. In the wake in the centerline, the deposition is less than to the sides so that the pattern looks like a horseshoe.

The impact of soil moisture on erosion was studied by Chepil (1956). They considered first the influence of soil water on cohesive forces. With increasing water content, the erodibility decreased. McKenna-Neuman et al. (1989) did a lot of wind tunnel measurements on the effect of soil moisture on threshold friction velocity. They proposed to better take moisture tension than moisture content to calculate the threshold velocity for wet soil as it is independent on grain size. Shao et al. (1996) collected also some data which agreed fairly well with the observations of McKenna-Neuman et al. (1989). The sand flux and also the dust entrainment rate rapidly decrease with increasing soil moisture content until it exceeds  $0.04 \text{ m}^3\text{m}^{-3}$ , then they predict the wind erosion to be practically zero.

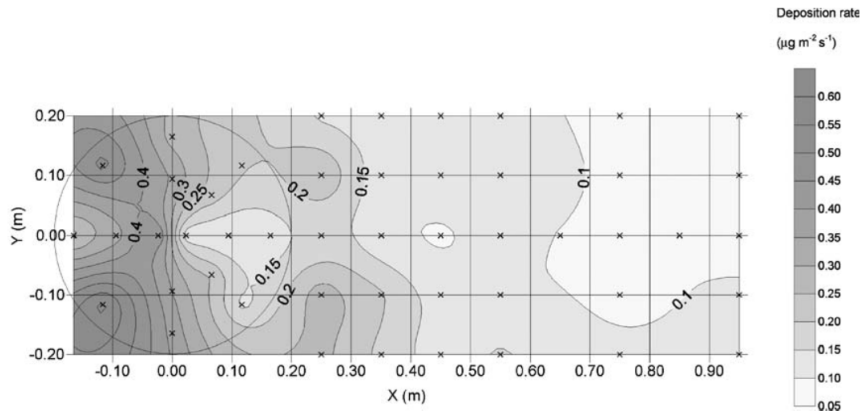


**Figure 2.1:** Contour plot of wind tunnel deposition rate ( $\mu\text{g m}^{-2}\text{s}^{-1}$ ) around the cone (center at  $x=0, y=0$ ). The darker the area, the higher the deposition rate. Increased deposition on windward face and around the cone, decreased deposition in the wake (Parker et al., 2004).

Not only the soil water content but also the moisture in the air plays an important role in wind erosion. Corn (1961) summarized the different researches studying the link between adhesion force and humidity at that time and concluded that relative humidity has a great effect on the adhesion forces but due to different theories, the nature of the influence was not clear. Ranade (1987) examined in his research the adhesion forces of small particles on surfaces. He also took condensation between bodies in account which causes an attractive force and found out that water vapour begins to condensate at a relative humidity of 65 to 70 %. In their research about particle bounceoff and resuspension rates, Wu et al. (1992) observed the effects of relative humidity to be greater at lower wind speeds. Kim et al. (2016) observed that the effect of relative humidity is the highest on hydrophilic particles on hydrophilic surfaces and the lowest on hydrophobic particles on hydrophobic surfaces. They also found the main change of resuspension to be in the range between 55 % and 70 %. The resuspension rates of glass particles on glass surfaces, for example, decreased by almost three orders of magnitude, whereas the effect on PE particles on glass was smaller.

## 2.2 Processes of particle transport

All of these factors control the erosion of a particle but the mode of transport is mainly controlled by the size fraction of the particle. Mineral particles can be divided into bigger particles down to a size of 1000  $\mu\text{m}$ , sand with a size  $> 60$  to 70  $\mu\text{m}$ , and dust with a size  $< 60$   $\mu\text{m}$ .

Particles larger than 1 mm in diameter are too heavy to be lifted in the air under normal atmospheric conditions but are instead pushed across the surface. The motion is called surface creep (Fig. 2.2). The momentum for the movement is received by the impact of saltating particles and the pressure of the wind (Shao, 2000; Bagnold, 1973).

Saltation is a bouncing motion of grains, mainly done by sand (Fig. 2.2). The size at which the particles rest on the surface despite the impact of other particles or the wind is the upper threshold of size for the sand fraction (Bagnold, 1973). The lower threshold is the size at which the upward currents get stronger than the downward velocity. The angle of the lifted particle is with  $55^\circ$  much larger than the angle of the impacting particle with  $10^\circ$  to the surface. The transporting distance of every bounce ranges from several millimeters to several meters. This mode is seen as the main transport mechanism of large quantities of sand particles as they can be moved from metres to kilometres in distance during an erosion event (Shao, 2000). The layer above the surface in which more than 75 % of the total mass flux is transported is called saltation layer (Ho, 2012) and can be several decimeter thick (Shao et al., 1999).

The dust fraction can get entrained in the air and remain there, which is called suspension in this context. Once they are suspended, they can get transported by the wind up to thousands of kilometers. As a further distinction, the term suspension can be divided in long-term and short-term suspension (Fig. 2.2). The former describes suspension of particles with a size of several microns up to  $20\ \mu\text{m}$ . These particles can remain in the atmosphere for several days. Particles in short-term suspension, usually  $20$  to  $70\ \mu\text{m}$  in size, are normally only several hours in suspension. Their transportation distance

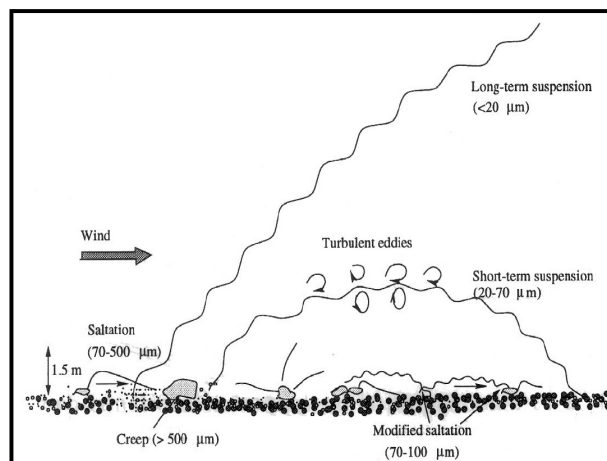


**Figure 2.2:** Different modes of particle transport: Creep, saltation and suspension. The latter can be further classified into short-term and longterm suspension (Shao, 2000).

hardly exceeds several hundreds of kilometers (Shao, 2000). When the carrying capacity of the wind isn't sufficient anymore, the particles deposit again.

A particle is influenced by a drag force and a resistive force. Depending on which force is greater, the particle will move or not. If the wind speed exceeds a certain velocity threshold, particle movement will start due to the direct fluid pressure of the wind. Bagnold (1973) called it *Fluid Threshold*. He also introduced the term of the dynamic threshold as the critical wind strength at which stationary particles start to move after the impact of other moving particles. As momentum is transferred from the moving particles to the surface and to the stationary particles, the dynamic threshold is lower than the fluid threshold. Thus, a particle either get entrained in the air by the aerodynamic lift or by the momentum of other saltating particles. The first case plays only a small role in reality because the erosivity of the wind, that is the potential ability of the wind to erode particles from the surface, is seldomly high enough due to the strong cohesive forces on small particles. The impact of saltating particles is much more effective (Shao et al., 1996).

The conceptual model by Rice et al. (1999) shows the probability distributions of the impact energy delivered to the surface,  $P[E_i]$ , and of the local surface strength  $P[E_s]$  (Fig. 2.3).  $E_i$  is due to the impact of saltating particles and is called the erosivity whereas  $E_s$  depends on cohesive forces such as capillary forces, Van-der-Waals forces or electrostatic forces. The area in the graph, where both tails overlap, defines the rate of erosion, that is the erodibility of the system. Hence, only the impacts with the most energy can erode particles from the surface that are bound in the system the weakest (Rice et al., 1999).

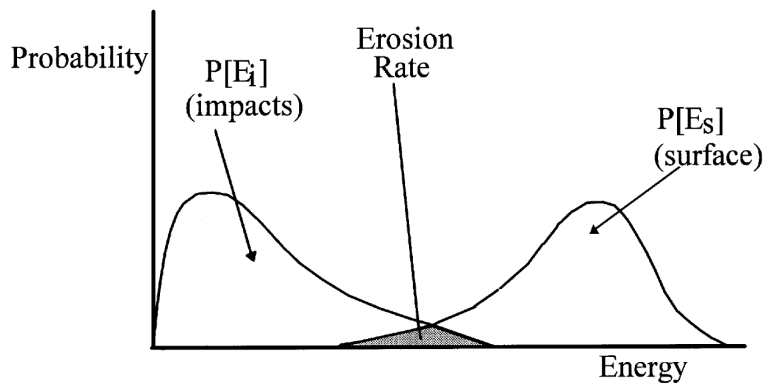


**Figure 2.3:** Conceptual model of crust erosion:  $P[E_i]$  describes the probability distribution of the impact energy to a surface,  $P[E_s]$  the probability distribution of the local surface strength (Rice et al., 1999).

The sand flow  $q$  over a surface can be scaled as follows (Bagnold, 1973):

$$q = C \sqrt{\frac{d}{D}} \frac{\rho}{g} V_*'^3 \quad (2.2)$$

Where:

- $q$ : sand flow ( $\text{g cm}^{-1} \text{ s}^{-1}$ )
- $C$ : empirical coefficient, depends on the type of surface (1)
- $d$ : grain diameter of the sand (mm)
- $D$ : grain diameter of a standard 0.25 mm sand (mm)
- $\rho$ : density of the fluid ( $\text{g cm}^{-3}$ )
- $g$ : gravity acceleration ( $\text{cm s}^{-2}$ )
- $V_*'$ : velocity gradient ( $\text{cm s}^{-1}$ )

Here, he assumed a cubic dependence on  $V_*'$ . However, Ho et al. (2011) showed in their research that there is a distinction between sand transport over an erodible and a rigid bed. Over a rigid bed, mean saltation length and horizontal particle velocity both increase with increasing wind speed whereas over an erodible bed, both values are independent of the wind speed. This is due to the fact that with increasing wind speed, the particle concentration in the saltation layer is also increasing but because of the higher friction between the particles, the particle speed remains almost unchanged. This invariance of saltation length with the wind strength leads to a quadratic dependence of air friction velocity on the saturated sand transport rate over an erodible surface.

Shao et al. (1999) observed two modes of saltation, a weak saltation and a strong saltation mode, with a critical lift-off velocity that separates the particles into these two modes. The motion in the first regime is similar to creep. Therefore, the particles in the strong saltation mode contribute more to the transport of sand and momentum. However, strong saltation only occurs at high friction velocities. In their research, particles being exposed to a friction velocity of  $u_* = 0.5 \text{ ms}^{-1}$  still entered the weak saltation regime.

In the strong saltation mode, the process of splashing plays an important role. Splashing describes the process of an impacting particle that rebounds and also ejects other particles from the bed. Beladjine et al. (2007) found out that the number of splashed particles depends on impact angle and velocity. However, the mean quadratic horizontal velocity is almost unaffected by changes of these two impact factors.

The lift-off velocity of the particles that are impacted by other particles is much larger than the critical lift-off velocity. It's a positive feedback process: The particles that are bombarded by particles in the strong saltation mode

also enter the strong saltation regime and have an impact on other particles.

Splashing is especially important at the initial stage of saltation when the friction velocity is large. As the saltation reaches an equilibrium and the friction velocity becomes smaller, splash likely becomes less important (Shao et al., 1999).

Concerning the critical friction velocity that is needed to lift the sand particles off the surface for saltation or suspension, Bagnold estimated a linear relation between particle diameter and friction velocity. However, the smaller the particles, the more the inter-particle cohesion forces increase. Greeley et al. (1985) derived an equation for this relation with functions for aerodynamic drag force and cohesive forces. Shao et al. (2000) modified this model into a simpler expression:

$$u_{*t}^2 = f(Re_{*t})(\sigma_p g d + \frac{\gamma}{\rho d}) \quad (2.3)$$

Where:

- $u_{*t}^2$ : squared threshold friction velocity ( $\text{m}^2\text{s}^{-2}$ )
- $f(Re_{*t})$ : function depending on Reynolds-number (1)
- $\sigma_p$ : particle-to-air density ratio (1)
- $g$ : acceleration of gravity ( $\text{ms}^{-2}$ )
- $d$ : diameter of the particle (m)
- $\gamma$ : parameter fitted to measurements ( $\text{kgs}^{-2}$ )
- $\rho$ : air density ( $\text{kgm}^{-3}$ )

They presented a comparison of their simpler expression 2.3 and the original Greeley-Iversen scheme as well as some data from other publications and plotted also a variation of  $\gamma$  of their equation (Fig. 2.4).

The equations agree fairly well for the particle size range of 50 to 1800  $\mu\text{m}$ . However, for the range smaller than 50  $\mu\text{m}$ , the difference increases. As there is no reliable data for this particle range, it is difficult to decide which equation performs better (Shao et al., 2000).

According to these equations, the threshold friction velocity for a sand particle with a diameter of 58  $\mu\text{m}$  would lie in the range of 0.2 to 0.3  $\text{ms}^{-1}$ . The density of 1  $\text{gcm}^{-3}$  of the MP spheres that were used for the experiments is lower than the density of quartz with 2.65  $\text{gcm}^{-3}$ . This difference in density may influence the critical friction velocity by lowering it. On the other hand, cohesion forces such as electrical forces might be greater and potentially increase the critical friction velocity.

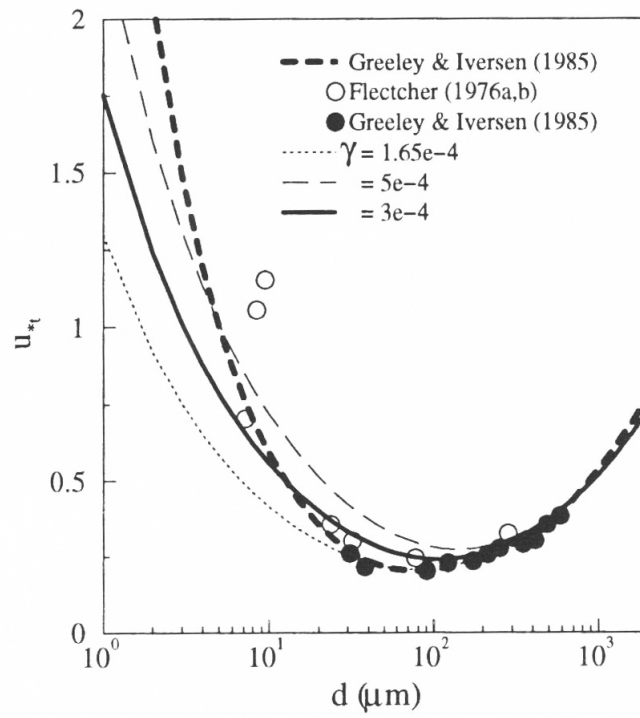


**Figure 2.4:** Comparison of the Greeley-Iversen scheme and the simpler expression of Shao with different values of the parameter  $\gamma$  concerning the calculation of the threshold friction velocity of a particle depending on its diameter. Additionally, previously observed data by Fletcher (1976a) and Fletcher (1976b) was added in white circles (Shao et al., 2000).

## 3. Materials and Methods

### 3.1 Microplastic particles

The MP particles used for this research were fluorescent green polyethylene particles with a size range between 53 and 63  $\mu\text{m}$  and a density of  $1.00 \text{ gcm}^{-3}$  (Cospheric, USA). One particle weighed on average  $0.102 \mu\text{g}$ , calculated by size and density. A polysorbate-type nonionic surfactant (Tween 20, Cospheric, USA) was used to dissolve the hydrophobic particles in water to use them for the spectrofluorometric method. Under the microscope, it could be seen that the reflection off the particles was not a perfectly round shape (Fig. 3.1), suggesting that the surface of the microspheres was not homogeneous but a bit rough. It could also be seen that the fluorescent film is not homogeneously distributed on the surface. There were brighter and dimmer parts on the surface.

The form of the MP particles was not varied across the experiments. Spheres were used for the experiments in order to gain basic knowledge of the transport processes as it is the most studied and best understood form.

The particle properties are summarized in table 3.1.

**Table 3.1:** Characteristics of the MP particles that were used in the experiments

Material	Form	Size	Weight	Density
Polyethylene	Spherical	53-63 $\mu\text{m}$	0.078 - 0.131 $\mu\text{g}$	$1.00 \text{ gcm}^{-3}$

### 3.2 The wind tunnel

The experiments were conducted in a wind tunnel, which features a three meter free stream section with 60 cm in depth and 120 cm in height. In the beginning of the wind tunnel, there is a HEPA filter installed, which prevents large particles to get sucked into the tunnel. Behind the filter, a section with pipes arranged as a honey comb are installed to parallelize the stream and to exclude external turbulence (Fig. 3.2).

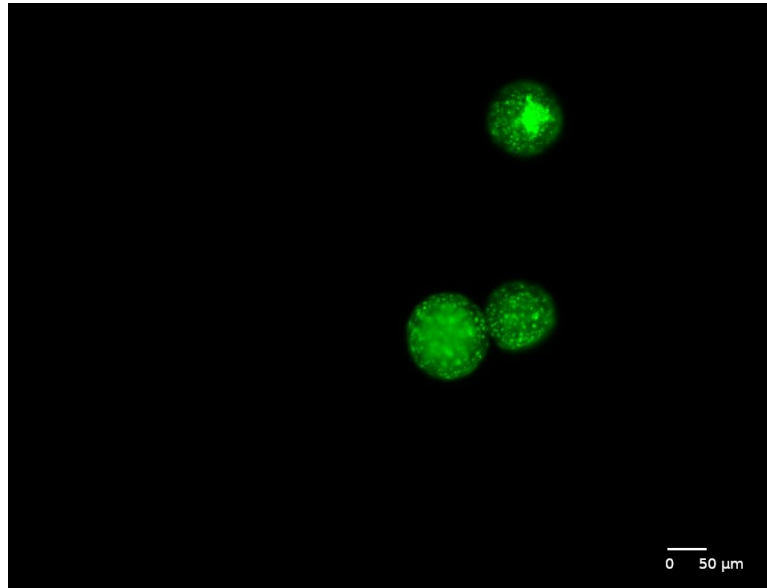


**Figure 3.1:** Three polyethylene particles, covered with a green fluorescent film, with a size of 55, 57 and 62  $\mu\text{m}$  under the fluorescence microscope (Leica DM 5500 Q, Leica Microsystems, USA)

After the free stream section, in the back of the tunnel, there is another HEPA filter which holds back the MP particles. Behind that, blades redirect the stream towards the fans.

The mapping of the wind speeds in the tunnel with these unmodified conditions showed that the air flow developed homogeneously in the wind tunnel, so the wind speed was relatively constant throughout the x-axis. The friction velocity at  $2.5 \text{ ms}^{-1}$ , the highest velocity measured, was around  $0.015 \text{ ms}^{-1}$  (Fig. 3.3).

The wind speeds at this setting, however, were insufficient to induce particle movement. The cross section of the wind tunnel was constricted to a size of 54 cm in height and 27 cm in width. The construction was built from extruded polystyrol foam as the material was inexpensive, light, and easy to work with. The contamination of the testing section with polystyrol particles can be excluded because the foam is very hard so that it is unlikely that small pieces break apart. Additionally, it is not fluorescent which is the main characteristic for the detection.

Besides higher wind speeds, more turbulence was needed in the tunnel. To change the ratio of velocity variance to mean wind speed, which is the turbulence intensity, some obstacles were built into the tunnel.

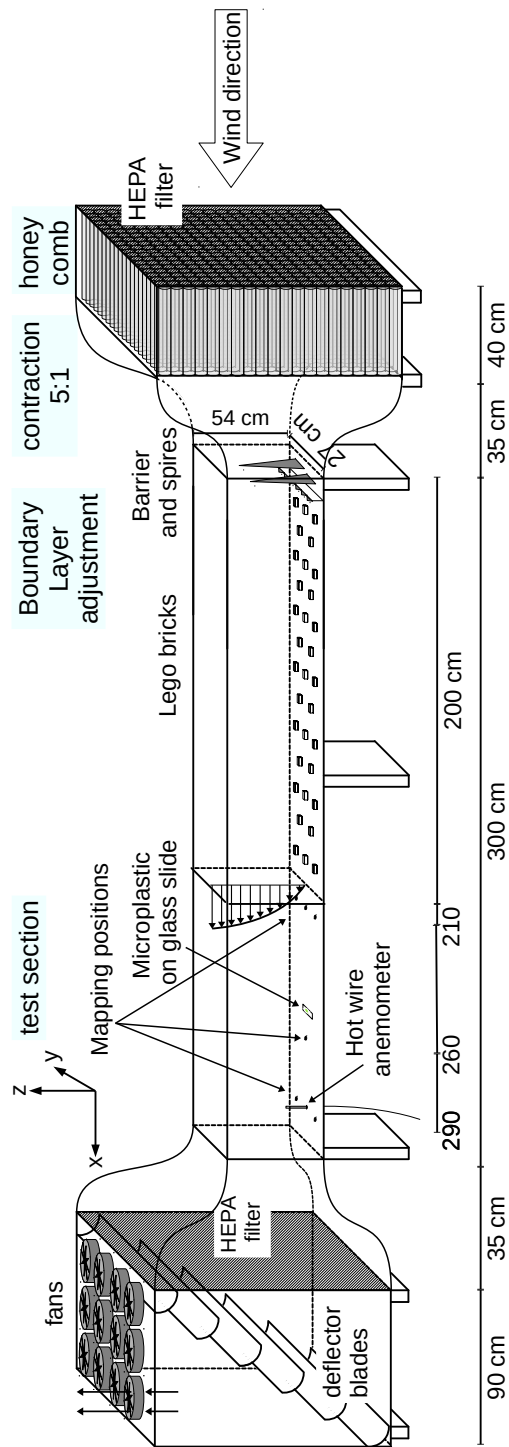


**Figure 3.2:** Scheme of the wind tunnel with adjustment (modified from L. Pfister, pers. comm.)

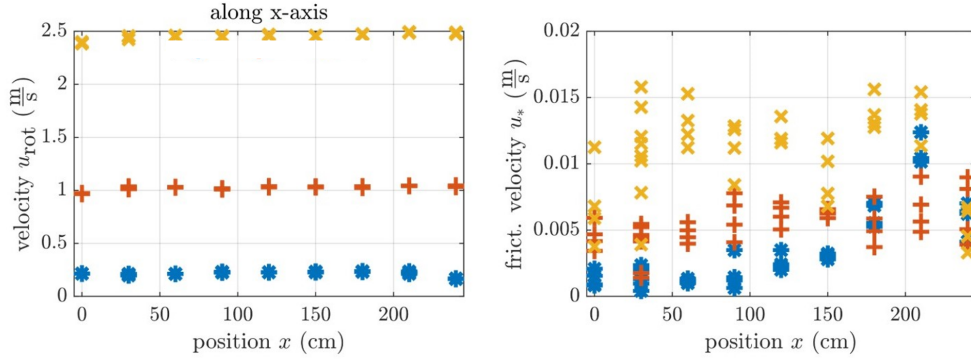


**Figure 3.3:** Wind tunnel mapping before adjustment at  $0.2$ ,  $1.0$  and  $2.5 \text{ ms}^{-1}$  (blue stars, red crosses, yellow Xs)(A. Freundorfer, pers. comm.)

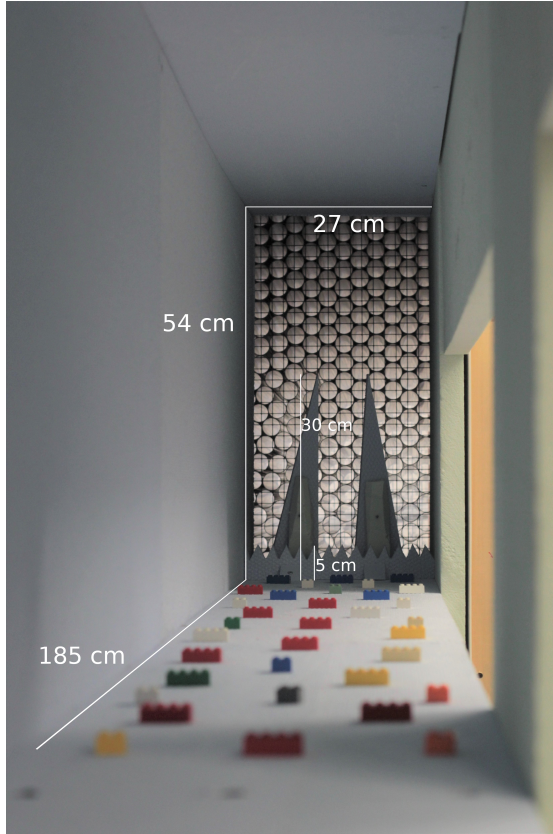


**Figure 3.4:** Photograph of the adjusted wind tunnel, taken from the back with view to the front

stream line ( $x = 2100 \text{ mm}$ ,  $x = 2600 \text{ mm}$  and  $x = 2900 \text{ mm}$ ) for three different

A thick boundary layer was created using two spikes that were installed in the first section of the wind tunnel with a height of  $30 \text{ cm}$  and a base of  $7.5 \text{ cm}$ ,  $4 \text{ cm}$  space in between and to the edges, followed by a smaller barrier with spikes on the top. The barrier is  $3 \text{ cm}$  high plus the spikes with  $2 \text{ cm}$  height and  $2 \text{ cm}$  width. The following section of  $185 \text{ cm}$  is covered with lego bricks as small roughness elements by  $5.8 \%$  of the surface area (Fig. 3.4). The construction was built according to work by Gromke et al. (2005) and Shojaee et al. (2014). These obstacles increased the momentum roughness length  $z_0$  as well as the velocity variance as more turbulent eddies were formed.

After the adjustment, there was still a free stream section of three meters. In order to map the new conditions, measurements were taken near the end of the free

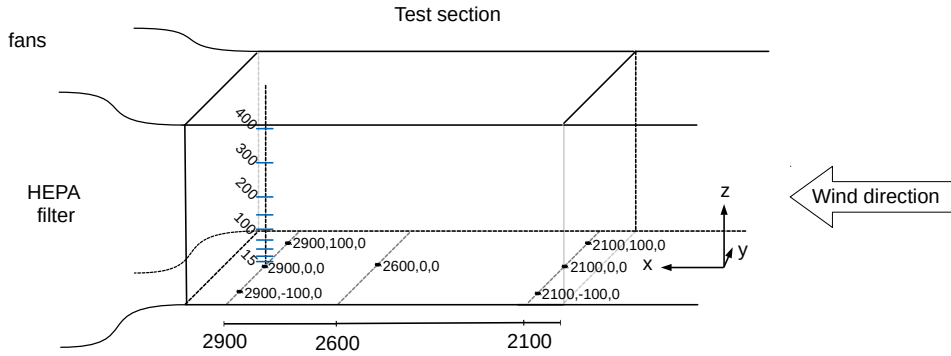


**Figure 3.5:** Scheme of the test section in the wind tunnel with the mapping positions.  $x = 0$  is defined as the beginning of the contraction zone, before the spires.  $x$  is in the direction with the wind stream.  $y = 0$  is defined as the centerline in the tunnel.  $z = 0$  is the surface of the tunnel.

fan speed settings (150 V, 175 V and 200 V). At the first and the last position ( $x = 2100$  mm and  $x = 2900$  mm), measurements ten centimeters to the left and to the right of the middle line were included to investigate the effects of the walls on to the airstream (Fig. 3.5). The wind speed was measured with a hot wire anemometer (TROTEC TA300 Anemometer, 1 Hz) at eleven heights (from the ground: 15 mm, 30 mm, 50 mm, 75 mm, 100 mm, 150 mm, 200 mm, 300 mm, 400 mm, 470 mm, 520 mm). The anemometer could be extended in height and was pushed through a little hole in the ground (Fig. 3.2). At position 470 and 520 mm, the ceiling impacted the airflow and thus, a reduction in wind speed was observed. Hence, these two positions were excluded in the wind profiles (Fig. 3.6 for fan configuration of 200 V)(other configurations can be found in the appendix).

Following Shojaee et al. (2014), it takes approximately six times the height of the spires downstream to develop the boundary layer. In this case, the spires were 30 cm high so the boundary layer should have developed after 180 cm. The boundary layer evolved nicely near the end of the free stream section, especially in the center (position:  $(2600,0,z)$ ) as the difference between data and logarithmic model is small (Fig. 3.6). The location  $(2100,100,z)$  has the highest deviation from the model. The wind speed at  $z = 400$  mm, approximately  $8 \text{ ms}^{-1}$ , is very high compared to the wind speed at the same height further down the tunnel with  $6.5 \text{ ms}^{-1}$  ( $2900,100,z$ ). On the other side of the tunnel at that height ( $(2100,-100,400)$  and  $(2900,-100,400)$ ), the wind speed is lower with  $6.4 \text{ ms}^{-1}$  and  $6 \text{ ms}^{-1}$ . This finding might be an indication for a slightly canalized flow to the left of the tunnel ( $y=100$ ).

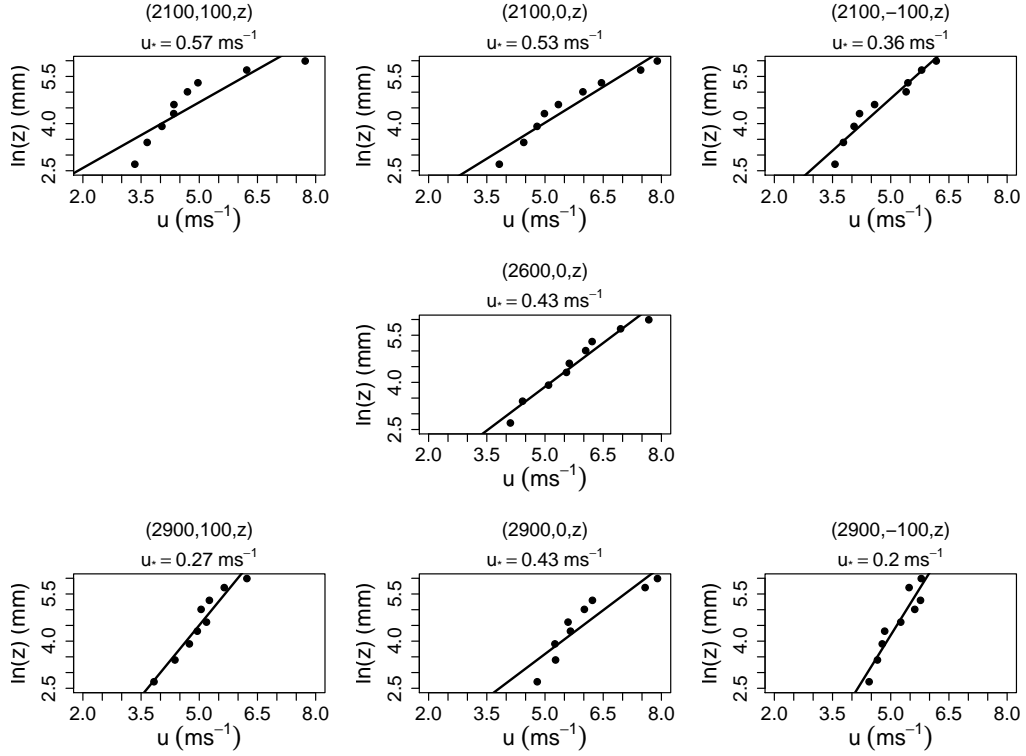


**Figure 3.6:** Logarithmic wind profiles at different locations in the adjusted wind tunnel (Fig. 3.2) at the wind tunnel setting of 200 V (unit of locations: mm). The plots are arranged from the top view of the tunnel.

As the measuring point at  $x=2600$  mm is the closest to the sampling area, the friction velocities are calculated with equation 2.1 of the logarithmic wind profiles at this location for wind speeds of the fan configurations of 100 V, 125 V, 150 V, 175 V and 200 V (Fig. 3.7). The friction velocity values vary from  $0.16 \text{ ms}^{-1}$  to  $0.43 \text{ ms}^{-1}$  and are higher compared to the pre-modified wind tunnel (Fig. 3.3). At a fan speed setting of 150 V for example, the friction velocity of the modified tunnel is  $0.32 \text{ ms}^{-1}$  compared to  $0.015 \text{ ms}^{-1}$  before the modification.

To compare wind speed and friction velocity, the wind speed measurements at the same downstream location are taken at a height of 150 mm. A  $R^2$  value of 0.987 shows that the linear model fits well to the data (Fig. 3.8). The velocity measurement uncertainty of the hot wire anemometer was  $0.1$  to  $0.2 \text{ ms}^{-1}$ . The data point at a wind speed of  $2.1 \text{ ms}^{-1}$  has the highest deviation from the linear model but it is still within the range of the measurement uncertainty.

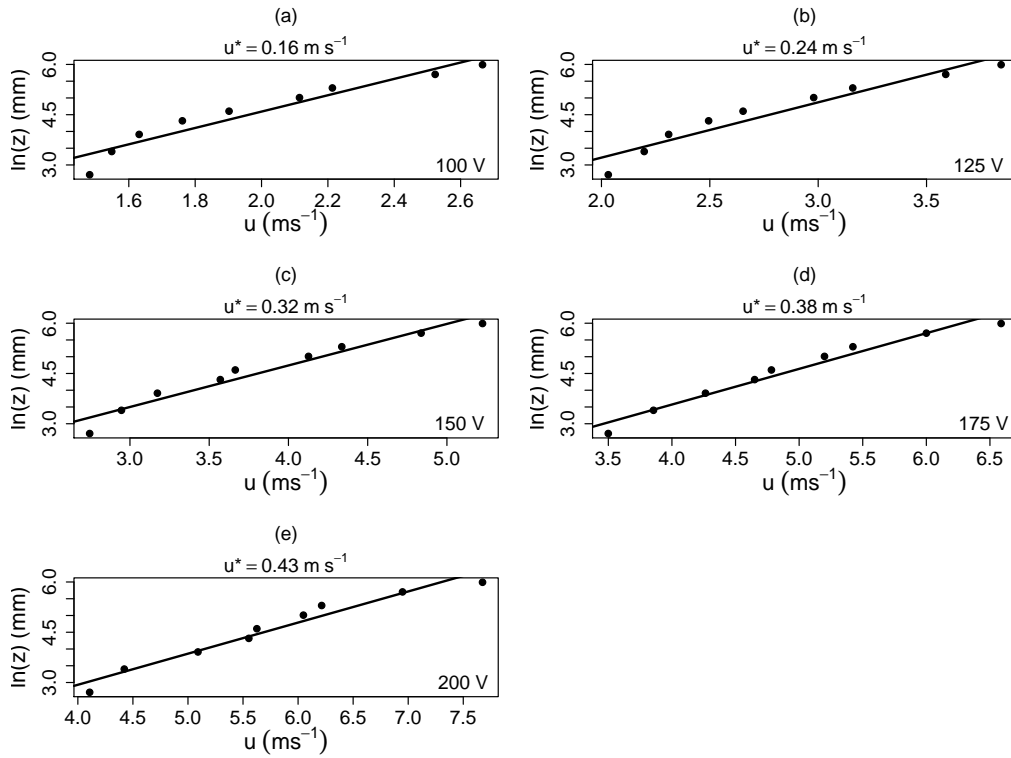


**Figure 3.7:** Logarithmic wind profiles for different fan speed settings ((a) = 100 V, (b) = 125 V, (c) = 150 V, (d) = 175 V, (e) = 200 V) at the same location in the wind tunnel (2600,0,z)(mm)

For the comparison of wind speed to fan speed settings of the wind tunnel (Fig. 3.9), the data of the later experiments are taken due to more wind speed values per fan speed setting (four wind speed values at each fan speed setting due to four different experiment lengths in the later experiments). The increase in wind speed with increasing power of the wind tunnel follows a linear model with a  $R^2$  value of 0.997.

Figure 3.8 and Figure 3.9 are important summaries for future studies in the wind tunnel.

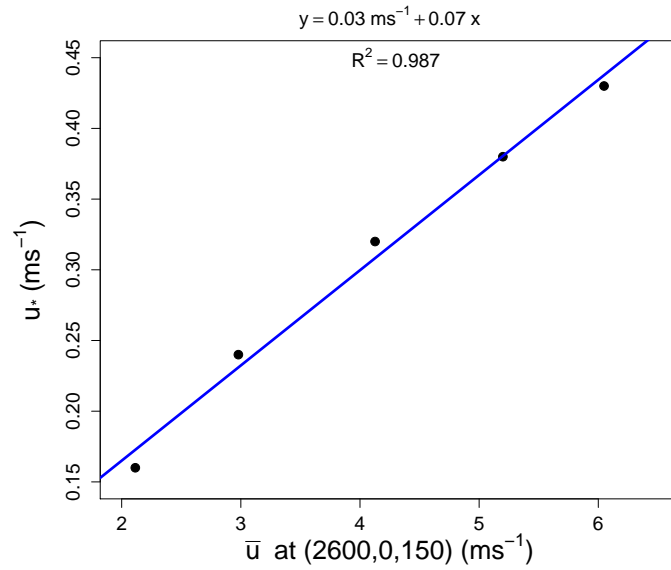


**Figure 3.8:** Relation between friction velocity and mean wind speed at (2600,0,150), measured during the mapping of the adjusted wind tunnel at 2 min intervals (Fig. 3.7).

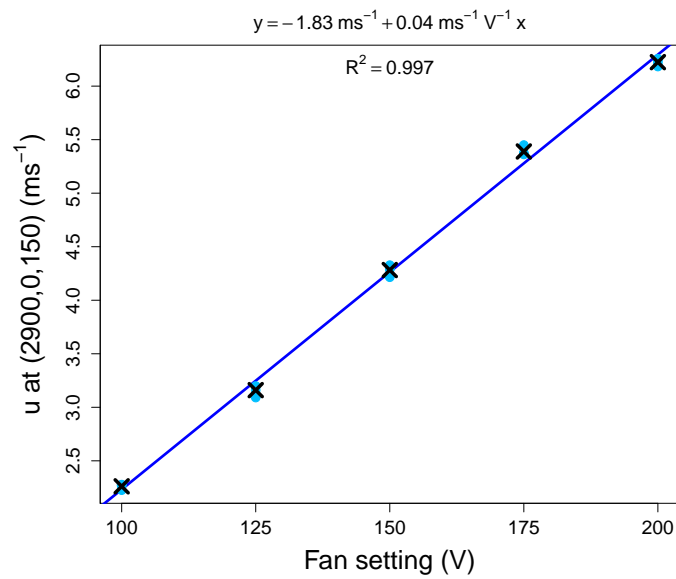


**Figure 3.9:** Wind speed values from experiment 13 to 32 (Table 4.2) at (2900,0,150) depending on the fan speed settings in the wind tunnel. The crosses represent the mean wind speed over the four values at each fan speed setting.

### 3.3 Methods to detect MP quantitatively

In this research, one research question was to find a suitable method to detect MP quantitatively in the wind tunnel. For this, three methods were tested: Fluorescence Spectroscopy, Fluorescence Microscopy and a photographic method. As none performed satisfactorily, a new method, the photometric method, was developed that combined the advantages of the others (Fig. 3.10).

All detection methods utilize the principle of fluorescence: According to Lakowicz (2006), a molecule leaves its ground state of excitation, when it absorbs light, and gets elevated to a higher, more excited state. Within the different states of excitation, there is another distinction between several levels of vibration. Having reached a higher vibrational level, the molecule rapidly relaxes to the lowest vibrational level of the first excited state. As this process takes place in  $10^{-12}$  s or less, it is shorter than the lifetime of fluorescence, which is near  $10^{-8}$  s and therefore already over as emission starts. As the molecule returns from the lowest vibrational level of the first excited state to any vibrational level of the ground state, it emits energy in the form of a photon. The emitted photons can be perceived as fluorescence light.

#### 3.3.1 Fluorescence Spectroscopy

For this detection method, the particles were dissolved in water using a polysorbate-type nonionic surfactant (Tween 20, Cospheric, USA). A solution with the surfactant was prepared to which the microspheres were added. With these dissolved particles, a  $500 \text{ mg l}^{-1}$  standard was made. To derive a calibration line, dilution series were made taking different volumes out of the standard solution. During pipetting, a magnetic stirrer was used in every flask to distribute the particles more homogeneously. Each of the dilution series contained concentrations of 200, 100, 50, 25, 10 and  $5 \text{ mg l}^{-1}$ , diluted in demineralized water in a volume of 20 ml. Every concentration of the three dilution series was filled in a cuvette containing 3 ml and was measured once with a fluorescence spectrometer (LS-55, PerkinElmer, USA) to get a calibration line. The microspheres were excited with a wavelength of 414 nm. The emission was recorded between 500 and 550 nm, whereas the peak of emission was at 504 nm. After subtracting the fluorescence value of the blank, which was demineralized water, a linear model was fitted to the data to get a calibration line between the concentration, which was the dependent variable, and the fluorescence value, which was the independent variable. To measure the correlation between these two variables, the Pearson correlation coefficient was used.

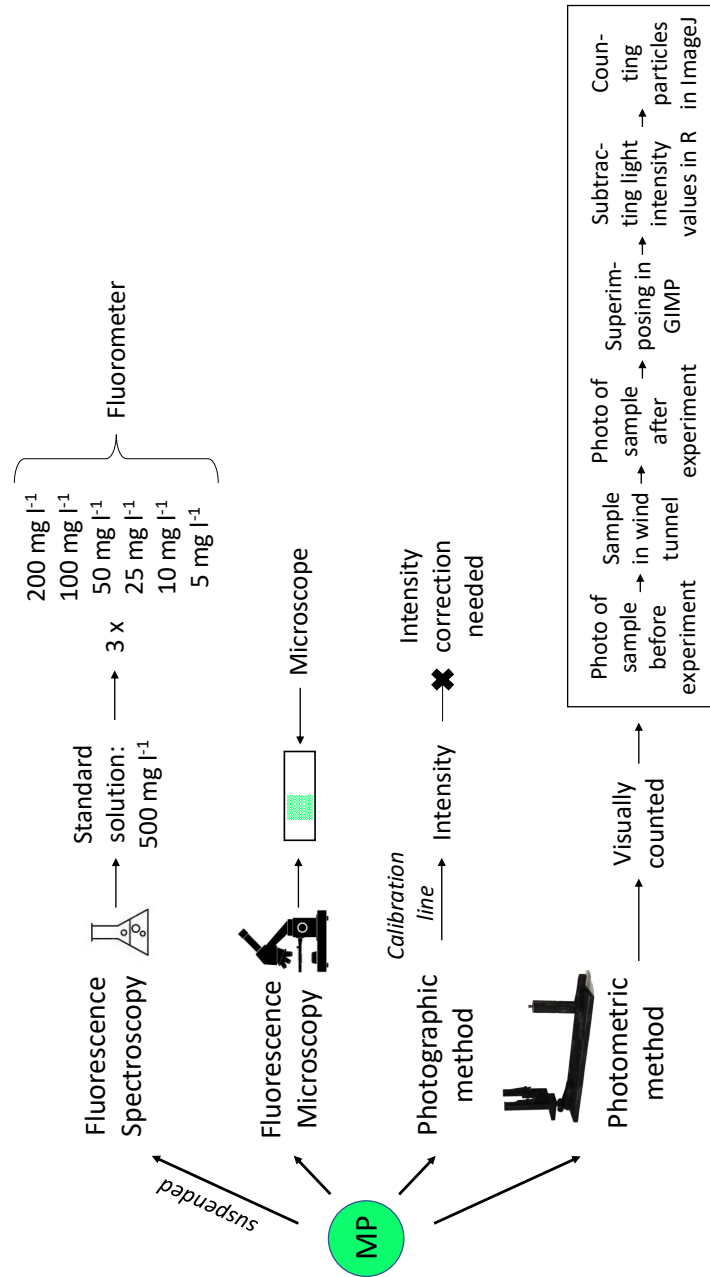


**Figure 3.10:** Three different methods were tested in this research: Fluorescence Spectroscopy, Fluorescence Microscopy and a photographic method using difference in light intensity of two photos due to a different number on particles on the sample. Eventually, a fourth method, the photometric method, was developed that counted the particles visually on the sample.

### 3.3.2 Fluorescence Microscopy

For this method, glass slides with MP particles were measured with a fluorescence microscope (Leica DM 5500 Q, Leica Microsystems, USA) and a filter cube (Leica I3, Leica Microsystems, USA), which has an excitation filter, a dichromatic mirror and a suppression filter built-in. Wavelengths between 450 and 490 nm can pass this excitation filter of the cube and reach the dichromatic mirror which reflects the light onto the sample due to its shorter wavelength. The emitted light of the sample is able to pass through the dichromatic mirror due to its longer wavelength and reaches the suppression filter which only passes wavelengths above 515 nm, which is green light.

In a first attempt, some particles were sprayed with a needle onto the glass slide which was covered with a non-fluorescent oil film. However, the particles overlapped and some particles were out of focus so they could not be counted. So either one uses the microscope's 3D capabilities to get a sharp 3D scan which enhanced the time needed for scanning and data storage volume compared to a 2D scan or the concentration and therefore density of the particles on the slide has to be lower to avoid an overlap of particles.

In a second attempt, only a small area of the glass slide, approximately  $1 \text{ cm}^2$ , was covered with particles using a sieve with a diameter of  $63 \text{ }\mu\text{m}$  to spray the particles more homogeneously onto the slide compared to using the needle. The number of particles varied from 850 to 15,000 particles per  $\text{cm}^2$ . After the scan, the particles were counted with an image processing software (ImageJ 1.52b). The software recognizes connected pixels of the same colour and counts it as one particle. Even though using a sieve, there were some clusters on the photo. The area of these clusters were then divided by the mean area of one particle to estimate the correct number of particles.

These measurements aimed to test the limit of this method as well as to compare the results with the photographic method in terms of accuracy of the scales as the particle number was also calculated using the weight of the particles on the glass slide.

### 3.3.3 Photographic method based on difference in light intensity

The last method that was tested used the difference in light intensity of photographs that were taken from glass slides with MP particles on the surface, which were excited by a UV lamp. A different number of particles on the sample resulted in a different light intensity in the photograph. An optical construction was built with which the glass slides could be photographed (Fig. 3.11). The distance between the glass slides and the camera must not

vary to always get the same segment onto the photograph. The materials for this construction were used from Thorlabs (Thorlabs Inc., USA). On the one side, the camera ((Canon EOS Rebel T3i, Canon, Japan) with an extension ring for macro photography (Minadax Automatik Zwischenringe, Impulsfoto, Germany) and a 50 mm lens (EF 50mm, f/1.8, Canon, Japan)) could be installed firmly and on the other side of the construction, there was a slide holder in which the glass slides were secured. The exposure was set to 10 seconds, f/8,0 and ISO 200. The white balance was set to tungsten light, that corresponds to a color temperature of around 3200 K. The whole construction was placed in a cardboard box that was sprayed before with a thermographic paint (HEWP-LT-MWIR-BK-11, LabIR, Czech Republic) with a high emissivity of 0.97 so that only the fluorescence of the particles was recorded. In the following, the cardboard box will be called Black Box. On the inside on the top, there was a UV lamp installed. The corners of the box were taped so that no light comes through. Different amounts of weighed MP were placed on the glass slides. After placing a sample into the slide holder, the box was shut and covered with a black foam while the photo was taken. The samples that were previously scanned at the microscope method were also photographed. The range of the examined number of particles varied from 20 to 73,000 particles per  $\text{cm}^2$ .

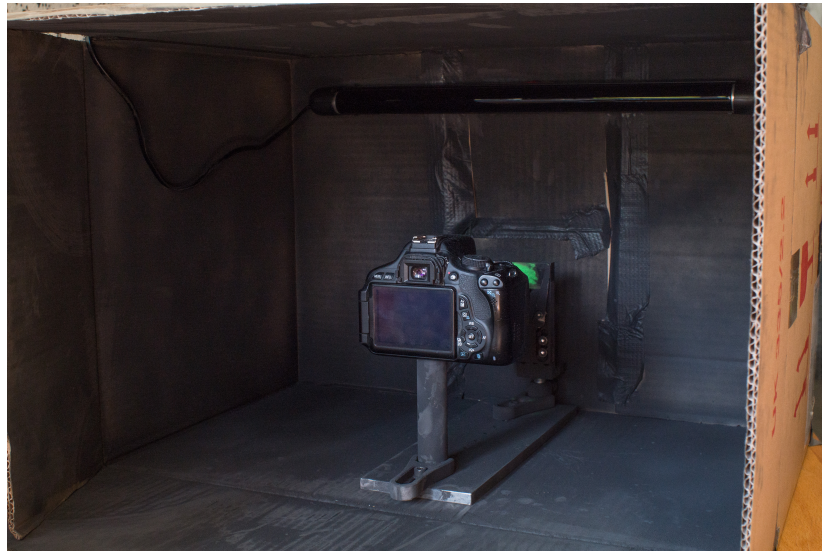


**Figure 3.11:** Optical construction with camera, slide holder and slide with MP particles, placed in the Black Box. On the top, the UV lamp is installed.

### 3.3.4 Visually counted MP with the photometric method

A novel method was developed to combine the advantages of the other methods. It uses the same construction as the photographic method (Fig. 3.11) but instead of determining the number of MP particles on the glass slide with light intensity, it counts the particles visually. Two photographs were taken of the same glass slide, one before the experiment in the wind tunnel and one afterwards. By processing these two photographs with different graphic and statistical computing softwares, only the particles that moved throughout the experiment could be visualized and counted (section 4.1.4).

## 3.4 Experiments on suspension and transport of MP in the wind tunnel

In order to ensure a developed boundary layer, the testing section was placed 2500 mm away from the beginning of the contraction zone in the wind tunnel.

The following parameters were varied wind speed ( $2.3 \text{ ms}^{-1}$ ,  $3.2 \text{ ms}^{-1}$ ,  $4.3 \text{ ms}^{-1}$ ,  $5.4 \text{ ms}^{-1}$  and  $6.2 \text{ ms}^{-1}$ , see Fig. 3.9), experiment length (1, 2, 4 and 8 minutes, including the time the wind tunnel needed to run consistently) and electrical charge using an ionizer (Benchtop Ionizer 212 v.2, B.E.STAT group, Germany). It was located parallel to the wind tunnel to reduce the differences in electrical charge in the laboratory. Unfortunately, there was no device available to actually measure the charge.

The reference wind speeds during the experiment were recorded by the hot wire anemometer at the location (2900,0,150) mm in the wind tunnel. The device measures three decimal places but the deviation from the reference velocity was about  $0.1 \text{ ms}^{-1}$  (Calibration test report). The turbulence intensity was calculated by the ratio of standard deviation and mean of the velocity.

The experiments are separated into block A, B and C (Table 3.2). Experiment block A was conducted on October 5th, block B on October 19th, and block C on October 25th. In experiment block A, wind speed and experiment length varied. The ionizer was irregularly turned on and off. In experiment block B, the ionizer was turned off for the whole experiment session and only wind speed and experiment length varied. The wind speed in experiment block C was set to  $6.2 \text{ ms}^{-1}$  but the experiment length still varied. One run of all four experiment lengths was done without the ionizer and two with ionizer. It was running two hours before the experiments started, turned off during the experiments but was turned on in between each experiment run for about two minutes.

For all experiments, previously weighed MP particles of 1 mg, which are

approximately 10,000 particles, were placed on glass slides before they were photographed in the Black Box. Then they were put in the wind tunnel. After the wind tunnel was shut down, the samples were taken out and photographed a second time to evaluate the two pictures with the photometric method. Table 4.2 includes the results of the MP experiments.

**Table 3.2:** Overview of different experiments that were carried out in this research with the experiment parameters that were changed

<b>Experiment parameter</b>	<b>Experiment A</b>	<b>Experiment B</b>	<b>Experiment C</b>
wind speed ( $\text{ms}^{-1}$ )	4.3, 5.4, 6.2	2.3, 3.2, 4.3, 5.4, 6.2	set to 6.2
experiment length (min)	1, 2, 4, 8	1, 2, 4, 8	1, 2, 4, 8
ionization	on off	off	on off

# 4. Results and Discussion

## 4.1 Results of the different methods

The unit of the concentrations of the different detection methods is particles per  $\text{cm}^2$ . The results using the original three methods are in the subsections 4.1.1, 4.1.2, and 4.1.3. These results motivated the development of the photometric method that was used throughout the experiments (subsection 4.1.4). This method was used to evaluate the experiments on MP suspension and transport (section 4.2).

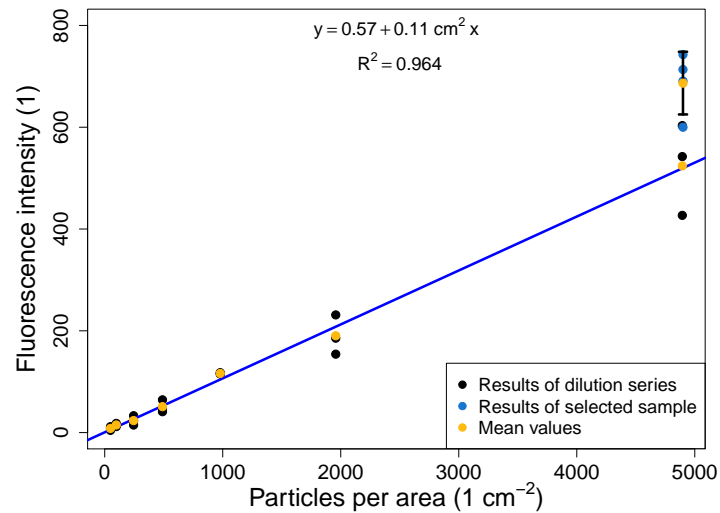
### 4.1.1 Fluorescence Spectroscopy

The fluorescence intensity for the three dilution series varied substantially (Fig. 4.1). At 250 particles per  $\text{cm}^2$ , it even varied with a factor of 2 (Fig. 4.1b). The measurement at 100 particles per  $\text{cm}^2$  of the second dilution series has been left out because the fluorescence intensity was 0.7 and therefore much lower than the intensity of the lowest value at 50 particles per  $\text{cm}^2$ . Therefore, it is likely an error.

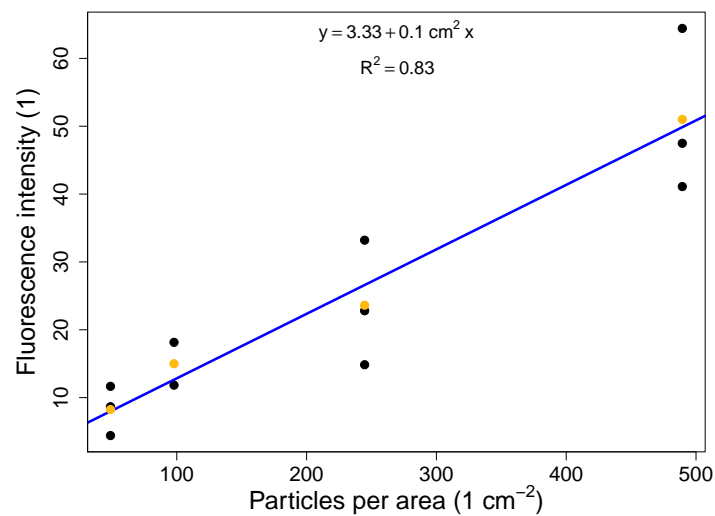
Nevertheless, the adjusted  $R^2$  value of 0.964 for the calibration line for all measurements is quite high. The linear equation shows an intercept of 0.57 fluorescence intensity units. Ideally, it should be 0 because the blank was already subtracted. For the calibration line for the low concentrations, the adjusted  $R^2$  value is only 0.83. The intercept is quite high with 3.3, especially considering that the lowest intensity value for 50 particles per  $\text{cm}^2$  is 4.5.

Because the offset was so high, one selected sample was tested several times in the same cuvette without any variation in order to quantify the random sampling error (Fig. 4.1a). The mean value in fluorescence intensity was evaluated for the four measurements taken from one sample. Even the measurements of this sample show a huge difference in fluorescence intensity. Overall, the intensity values for 5,000 particles per  $\text{cm}^2$  varied from 430 to 740, which corresponds to a factor of approximately 1.7.

The results for the method using fluorescence spectroscopy show a high deviation not only between the different solution series at each concentration but also when testing one sample multiple times.



(a) Full range of measured concentrations: 50 to 5,000 particles per  $\text{cm}^2$



(b) Only small concentrations: 50 to 500 particles per  $\text{cm}^2$

**Figure 4.1:** Calibration lines of the fluorometer (LS-55, PerkinElmer, USA) for polyethylene spheres with a diameter of 53-63  $\mu\text{m}$  and concentrations of 50 to 5,000 particles per  $\text{cm}^2$

The following problems were experienced when testing this approach, which may impact the estimates:

- Difficult to dissolve the MP particles

- Inhomogeneous distribution of the particles in the solution
- Particles sticking to the glass
- Loss of particles due to pipetting

As the microspheres are hydrophobic, the first problem was to dissolve them in water. Even after applying the surfactant, some particles were still located on the surface of the solution.

Even though most of the particles were dissolved, some of them remained unsuspected or sank to the ground after a couple of minutes. They moved around in the cuvette, so that also the results from several measurements of the same sample differed because the location of the particles had already changed again at the following measurement.

The particles adhered not only on the glass but also on the pipette for preparing the dilution series. So every time, the pipette touched the solution, some particles remained on the outside as well as on the inside of the pipette. As a result, on one side, the concentration of the first standard was reduced every time a pipette dipped in the solution, on the other side the concentrations of the dilution series might be not exact. Therefore, an overestimation of particles in every concentration standard is assumed.

Regarding the limits of this method, the lower threshold was reached in this test. Theoretically, diluting the  $5 \text{ mg l}^{-1}$  concentration one more time at a 1:10 ratio would produce a  $0.5 \text{ mg l}^{-1}$  dilution with five particles per  $\text{cm}^2$ . Due to the high variability and all the problems mentioned above, it cannot be assured that there is even one particle in the testing section. This concentration was also measured but the error was too high to detect a signal of fluorescence. The upper limit can be extended, however, the more particles there are in the cuvette, the more they might obscure each other in the view pane of the fluorometer and reduce the signal.

The most substantial problem for this method was that the particles did not suspend homogeneously. Hence, exact dilution concentration cannot be assured and the difference in the data is so high. The results and the problems showed that the reproducibility and the accuracy of this method are relatively low compared to the other two methods.

Concerning the practicability, the particles had to be dissolved first which needs a bit of preparation. The fluorometer has to warm up several minutes before it can be used. The measurements themselves only take a couple of seconds.

### 4.1.2 Fluorescence Microscopy

The number of particles of the scanned samples aligns very well with the number of particles calculated by dividing the total mass of used MP by the particles mean mass, with a slope from the linear model of 0.93 (Fig. 4.2). The deviation from the linear model and also the intercept of 111 are well within the measurement's uncertainties.

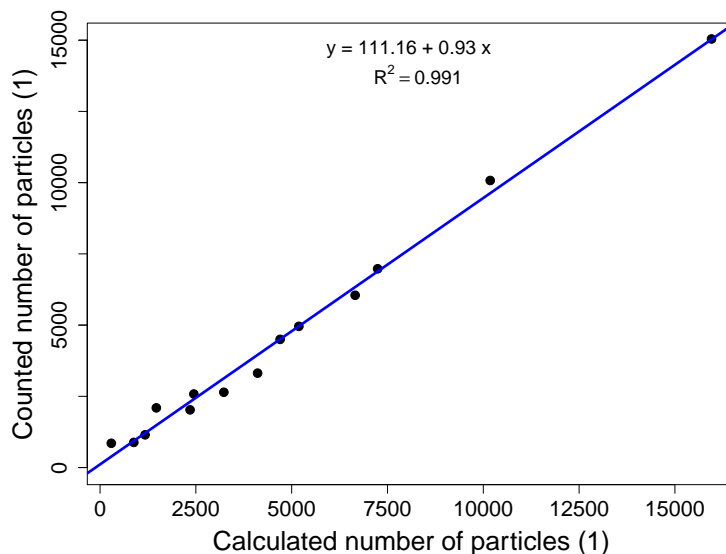


**Figure 4.2:** Comparison of number of MP particles on glass slide calculated by weighing the slide and dividing the total mass of used MP by the particles' mean mass and number of counted MP particles of the same slide under the microscope

At lower particle masses and therefore lower total mass of MP on the glass slide, the relative error is higher than at higher masses (Fig. 4.3). Especially the smallest mass of 30  $\mu\text{g}$  has the highest relative error. This finding is due to the ratio of 853 counted particles to the calculated number of 300 particles. As there are so few particles on the glass slide, the relative deviation is the highest.

Some issues have to be considered in further implementations of this method. First, the particles have to be sprayed over the surface homogeneously, otherwise, the particles overlay and some are not in focus, so the precise number of particles could not be determined. That is why this method is more precise the less particles are on the slide to scan. The higher the concentration, the higher is the probability to have an overlay of particles. However, that saturation is not reached yet with 15,000 particles per  $\text{cm}^2$  as the deviation from the calculated number is low (Fig. 4.2).

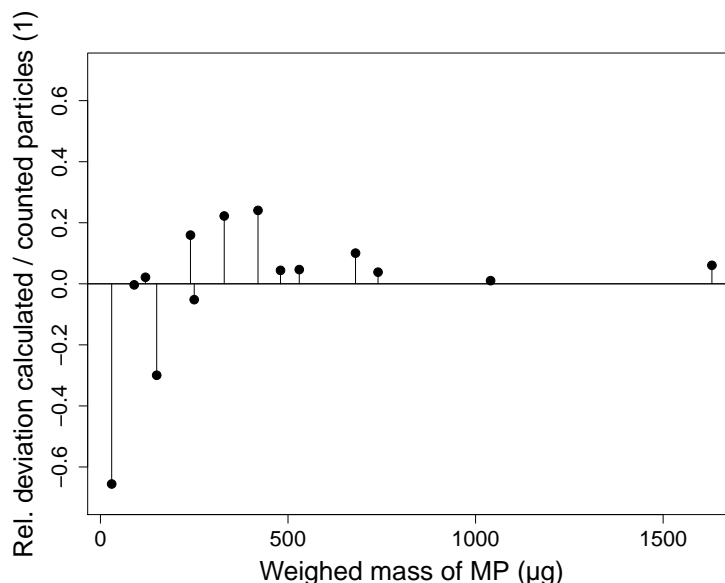


**Figure 4.3:** Different samples with varying total mass of MP were examined under a microscope and counted by the program Fiji. The number was also calculated by dividing the total mass of MP per slide by the mean mass of one MP particle. The difference of these two numbers is plotted relative to the number of the counted particles, represented by the zero line.

Second, this method is more time consuming than the other two because the laser has to warm up before the measurements and the scan itself takes some time. To measure an area of one  $\text{cm}^2$  with one channel, that is only one excitation wavelength, it takes about 10 minutes to scan one slide in 2D. The files that were produced were several Gigabyte large because one scan consisted of multiple single scans of a small area. In this case, 441 photos were put together to one picture. The data take some time to transfer and a computer with more than 4 GB RAM is needed to work with it.

As a result, this method is less practical than the other methods as time needed to process one sample is the highest. Nevertheless, the range that can be measured with this method is surprisingly large. The error will be higher the more particles per area are scanned but the image processing software could even count 15,000 particles per  $\text{cm}^2$  very accurately as it can be seen in comparison with the calculated number from the scales (Fig. 4.2). The largest benefit of this method is its preciseness, especially for small concentrations as the particles can be counted easily.

This method is can be used to scan some samples but it is not useful for a large number of samples. As it worked well in general, the same principle but with simpler handling, was used for the third method.

### 4.1.3 Photographic method based on difference in light intensity

For this method, the light intensity of a photograph of a sample with MP particles serves as an indicator for the number of particles on the sample. A calibration curve was needed as a reference. The model that was used for the calibration curve was the Michaelis-Menten equation (equation 4.1) as it was expected that the fluorescence intensity of the particles would follow a saturation curve (Cook et al., 2007):

$$v = \frac{V_{max}A}{K_m + A} \quad (4.1)$$

Where:

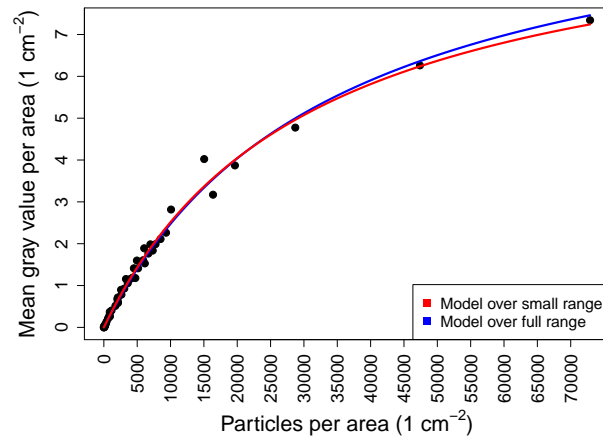
- $v$ : velocity of the reaction (mols<sup>-1</sup>)
- $V_{max}$ : maximum rate (mols<sup>-1</sup>)
- $A$ : substrate concentration (moll<sup>-1</sup>)
- $K_m$ : Michaelis constant (moll<sup>-1</sup>)

In this case,  $v$  is the light intensity value per area and  $x$  is the number of particles per area. Two different models were plotted to the data (Fig. 4.4). The parameter  $V_{max}$  for the blue model is 10.4 cm<sup>-2</sup> and  $K_m$  is approximately 31.300 cm<sup>-2</sup> and represents the particle concentration at the half of the maximum intensity value.

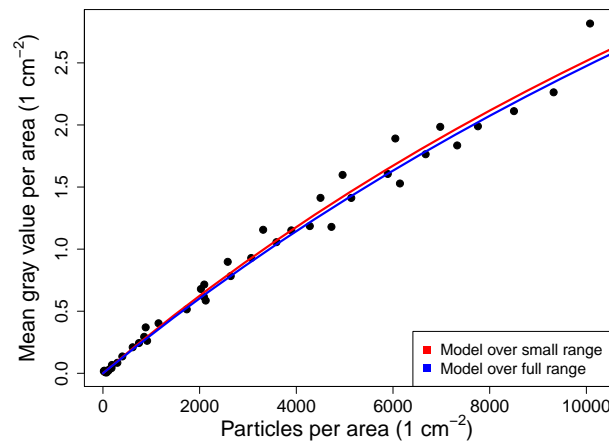
To compare the full and the small range of concentrations, the latter is plotted in Figure 4.4b. The parameters of the red model only for the smaller values are slightly different from the blue model:  $V_{max}$  is 11.6 cm<sup>-2</sup> and  $K_m$  is approximately 31.900 cm<sup>-2</sup>

The two models are very similar that means that this method is useful for low as well as for high concentrations. Even at the very high concentration of 73,000, the saturation was not reached yet. So this method could be useful for higher concentrations. In this research, it is more important to detect the smaller concentrations for the suspension of the MP particles.

As it was realized during the experiments, the intensity values differed from photo to photo as a result of varying light intensity in the photos themselves and less as a result of particle movement. This finding could be due to the light of the UV lamp which might vary in intensity or due to a different distance between glass slide and light source. The lamp was mounted on the ceiling of the box. The camera and slide holder were mounted on the base plate and may have moved between photos as the construction had to be taken out to change the slides. Another reason could be that some light was coming through the box even though it was covered with black foam. The settings of the camera stayed the same. These issues motivated a change to the photometric method.



(a) Comparison of the two models for particle concentrations of 20 to 73,000 particles per  $\text{cm}^2$



(b) Comparison of the two models for lower particle concentrations (20 to 10,000 particles per  $\text{cm}^2$ )

**Figure 4.4:** Light intensity data of MP particle samples that were put in the Black Box and were excited by an UV lamp. The data of the samples that were scanned under the microscope are also included. The blue model was fitted to the full range of data (20 to 73,000 particles per  $\text{cm}^2$ ), the red model only to the lower concentrations (20 to 10,000 particles per  $\text{cm}^2$ )

#### 4.1.4 Photometric method

As a fourth method, a photometric method was developed and tested. Two photographs were taken from one glass slide with previously weighed MP on

the surface using the slide holder of the construction in the Black Box (Fig. 3.11 and Fig. 4.5). One photograph was taken before the glass slide was deployed in the wind tunnel and one was taken after the experiment. These two photographs were processed with a graphic program (GNU Image Manipulation Program, 2.10.6) to align them with each other.



**Figure 4.5:** Close up of the construction for the photometric method: slide holder on the left, camera thread on the right, everything sprayed with a thermographic paint (emissivity of 0.97). The base plate ensures that the distance between sample and camera stays the same.

The second step was subtracting the green values with the statistical computing software R (RStudio, Version 1.0.136). The intensity values of each pixel of the photograph after the experiment were subtracted from the values of the picture before the experiment. Positive values match with particles that were blown away and were not on the same spot after the experiment, whereas negative values match with particles that appeared on a spot where there were no particles before (Fig. 4.6).

Under the assumption that there is no gain of microplastic particles from the front of the tunnel, the absolute positive value should be higher than the absolute negative value because the particles can either move on the glass slide and get counted as a positive and negative particle or they can be blown off the glass slide and get counted only as a positive particle.

As the light intensity had a range from -100 to 100 %, the threshold was set to 40 % to the positive and to the negative to remove the noise that arose from the different light intensities of the two pictures and to visualize only the particles that moved. New pictures were processed with only the

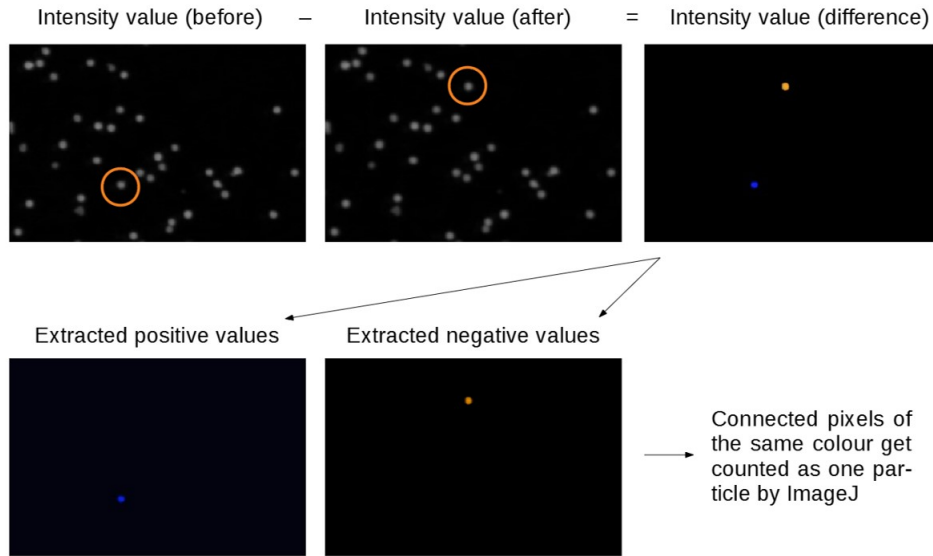


**Figure 4.6:** Scheme of evaluation of the photometric method: The intensity values of the photograph before and after the experiment get subtracted to extract the single particles that moved throughout the experiment (Software: GNU Image Manipulation Program 2.10.6). Subsequently, the particles on the new pictures get counted by an image processing software (ImageJ 1.52b)

positive and the negative values, respectively. The final step was to evaluate the new pictures with an image processing software (ImageJ 1.52b) that counts connected pixels of the same colour as one particle.

The applicability of this method was tested in the MP experiments in the wind tunnel and worked perfectly.

#### 4.1.5 Comparison of the different methods

During testing of the different methods, each method showed some advantages and disadvantages (Table 4.1).

**Table 4.1:** Comparison of the measurable MP particle concentration, the preciseness and the practicability of the different methods that were tested. The values in brackets are the theoretical limits of the methods.

Method	Tested range	Preciseness	Practicability
Spectroscopy	50 - 5000	low	middle
Microscopy	(0-) 850 - 15000	highest	low
Photography - Light intensity	20 - 73000	high	high
Photography - Visual approach	(0 - 15000)	high	high

Suspending the particles and measuring them in the fluorometer was difficult as the particles were hydrophobic. Even with applying the surfactant, some particles remained unsuspended so the results of the dilution series varied a lot. Due to the inhomogeneous distribution in the volumes, the number of particles in the cuvette could not be determined exactly. Without adjustments to the method (chapter 5), it cannot be used to study particle movement in the wind tunnel.

The microscopic method performed very well even at high concentrations but it is time consuming. The lower measuring limit of this method would be 0 particles per  $\text{cm}^2$  but this concentration could not be reached during the preparation of the samples.

As the light intensity of the particles differed between the photos, the photographic method could not be used.

Hence, the photometric method was developed. By combining the preciseness and the high measuring range of the microscope with a much simpler handling, this method is the most suitable for detecting suspension of MP particles from the glass slides in the wind tunnel. It is possible to visualize single particles moving with this visual approach by comparing two photographs and only count the moving particles, which is the implementation in this study.

#### 4.1.6 Recommendations to improve the methods and the experimental setup

Some problems occurred during the testing of the different methods. In this following section, my recommendations are collected to improve the methods and the experimental setup in further wind tunnel studies.

**Fluorometer:** To improve this method, the particles could be weighed before and put into the cuvette itself. That would prevent edge effects and uncertainties of the pipetting. To get them dissolved in the cuvette, they could be covered with a hydrophilic layer before. Another idea is to reduce the particles to smaller pieces as they would distribute more homogeneously in the solution. The calibration line would be different because the fluorescence intensity probably would differ compared to larger particles due to the increased surface. Therefore, the calibration line is only valid for the microspheres prepared the same way and not for their original size.

**Photographic method:** The results using the light intensity looked promising. To get the best results, the box has to be completely shut off the light. It is also necessary that the distance between the camera and the slide does

not change as the focus range with an extension ring is very small. As another feature I would suggest to also implement the light source in a stable construction because in this research, the construction had to be taken out of the box to change the slide. This could lead to a different distance from the slide to the light source. This way, the intensity could vary in the photo. Hence, a box with an opening on the top could be nice, being able to leave the construction in the box but to just change the slide. It is also important that the light source is constant during the experiments that the variation in light intensity on the photograph is as small as possible. Another way would be to determine a certain light intensity for the pictures so that it does not vary. This way, the changes due to particle movement could be noticed easier.

**Photometric method:** For the photometric construction itself, inserting the slide horizontally instead of vertically in the construction could improve the results as there is no guarantee that the particles do not slip on the slide or fall off especially with less electrical attraction forces. One way would be to turn the whole construction by  $90^\circ$  so that the side of the slide holder would be the base. The different angle from the lamp to the slide has to be considered because the different angle from slide to the light source could cause disturbing reflections on the slide. For the evaluation of the experiments, there are currently three programs needed (GIMP, R, ImageJ). The first step of laying the photographs exactly above each other could be excluded by having a completely fixed position of the glass slide. In this study, it was put into a slide holder which had a bit of a range in positioning the slides. With this adjustment, the method could be simplified even more.

**Experiments in the wind tunnel:** In the MP experiments, different samples were used for each experiment. The error that arose from this methodical decision (section 4.2.1 and Table 4.2) could be reduced by using just one sample. After one minute of experiment length, it could be put into the wind tunnel again with another run of one minute to see if there is a change in movement. That could be repeated for in total four and eight minutes. Like this, the result for eight minutes should be the same as for four minutes as the conditions of the slide and the deviation of the particles did not change. It should be ensured that during the time, the wind tunnel is turning on, the sample should be covered and only be exposed to the stream when the correct wind speed has reached. This could be constructed with a cover that could be removed from the sample by pulling it up with a cord from outside of the tunnel.

## 4.2 Results of the experiments on MP suspension

As the ionizer was used irregularly in experiment block A, it won't be discussed in particular but will be compared with experiment block C regarding the influence of the ionizer. Experiment block B and C provided more systematical results. The results of all experiments are shown in table 4.2. Concerning the terminology, moved particles are the positive particles that are at another location on the photo after the experiment. The particles that are blown away do not appear on the photo after the experiment. These particles are the difference between positive and negative particles as they are a part of the set of the positive particles but not of the negative particles.

### 4.2.1 Impact of wind speed on MP suspension

One expectation for the experiments on the impact of varying wind speed was to see a positive correlation of particle movement with rising wind speed. Rice et al. (2001) examined the effect of saltating particles on soil surfaces and they observed a decrease in the rate of erosion over time. This decrease already started within the first four minutes. Hence, the second expectation was to see such a trend in these experiments. The third outcome should be to set up the velocity range of the critical friction velocity for this setup and then compare it with the critical friction velocity for a sand grain of the same diameter.

Experiment block B (experiment name 13 to 32, Table 4.2) was conducted to systematically examine the impact of wind speed on the suspension of MP particles from the glass slides.

Experiment 19 (experiment length: 4 minutes) shows some surprising values. There are more than 4 times more particles moved than at an experiment length of 2 minutes. Higher turbulence intensity or higher wind speed cannot explain this behavior as both values are even a bit smaller than at experiment 18 (experiment length: 2 minutes).

At experiment 25 (experiment length: 1 minute), the number of positive particles (moved particles) is the highest for this wind speed, even higher than at experiment 28, which was conducted at 8 minutes experiment length. At experiment 26 (experiment length: 2 minutes), not even a quarter of the particles was blown away than at 1 minute. Again, the values for wind speed and turbulence intensity don't give an explanation. The number of the positive particles of experiment 25 and 28 is even higher than of experiment 29 and 32, despite lower wind speed.

**Table 4.2:** Results of all MP experiments of this research. The experiments are numbered: 1 to 12 were collected as experiment block A (ionizer irregularly turned on and off), 13 to 32 as experiment block B (ionizer off) and 33 to 44 as experiment block C (33 to 36: ionizer off, 37 to 44: ionizer on). The third column describes the setting of the fans in the wind tunnel and the experiment length. The fourth and fifth column show the numbers of positive particles and negative particles which were evaluated with the photometric method. The mean wind speed  $\bar{u}$  was calculated with the reference data of the hot wire anemometer over the experiment length. The turbulence intensity was calculated by the ratio of standard deviation of the velocity to mean wind speed of the experiment.

ExpBlock	ExpName	Volt_min	No. of pos. part. (1)	No. of neg. part. (1)	$\bar{u}$ (ms <sup>-1</sup> )	TurbInt (1)
A	1	150V_1min	23	45	4.332	0.0056
A	2	150V_2min	55	35	4.28	0.0111
A	3	150V_4min	31	16	4.23	0.0155
A	4	150V_8min	145	164	4.201	0.0142
A	5	175V_1min	384	261	5.529	0.0173
A	6	175V_2min	22	16	5.412	0.0172
A	7	175V_4min	97	24	5.422	0.0146
A	8	175V_8min	454	371	5.429	0.0139
A	9	200V_1min	220	77	6.408	0.0254
A	10	200V_2min	310	117	6.386	0.0215
A	11	200V_4min	895	303	6.372	0.0121
A	12	200V_8min	654	154	6.327	0.0122
B	13	100V_1min	0	0	2.226	0.0264
B	14	100V_2min	2	2	2.276	0.0219
B	15	100V_4min	3	3	2.278	0.015
B	16	100V_8min	4	4	2.267	0.0172
B	17	125V_1min	1	1	3.091	0.0147
B	18	125V_2min	3	2	3.199	0.0212
B	19	125V_4min	20	14	3.191	0.019
B	20	125V_8min	8	3	3.16	0.0182
B	21	150V_1min	8	5	4.328	0.0195
B	22	150V_2min	22	22	4.297	0.0144
B	23	150V_4min	10	12	4.288	0.0129
B	24	150V_8min	16	22	4.215	0.013
B	25	175V_1min	83	68	5.45	0.0165
B	26	175V_2min	15	8	5.369	0.0091
B	27	175V_4min	16	10	5.362	0.0115
B	28	175V_8min	62	38	5.377	0.0124
B	29	200V_1min	79	26	6.256	0.018
B	30	200V_2min	66	48	6.24	0.0107
B	31	200V_4min	89	39	6.217	0.0125
B	32	200V_8min	47	17	6.183	0.0113
C	33	200V_1min	41	17	6.205	0.0114
C	34	200V_2min	41	34	6.24	0.0103
C	35	200V_4min	34	21	6.193	0.011
C	36	200V_8min	39	20	6.261	0.0119
C	37	200V_1min	14	25	6.409	0.0149
C	38	200V_2min	38	12	6.29	0.0115
C	39	200V_4min	45	35	6.35	0.0135
C	40	200V_8min	47	26	6.2	0.0114
C	41	200V_1min	22	16	6.306	0.0094
C	42	200V_2min	20	21	6.272	0.0113
C	43	200V_4min	30	17	6.261	0.0109
C	44	200V_8min	20	13	6.277	0.0108

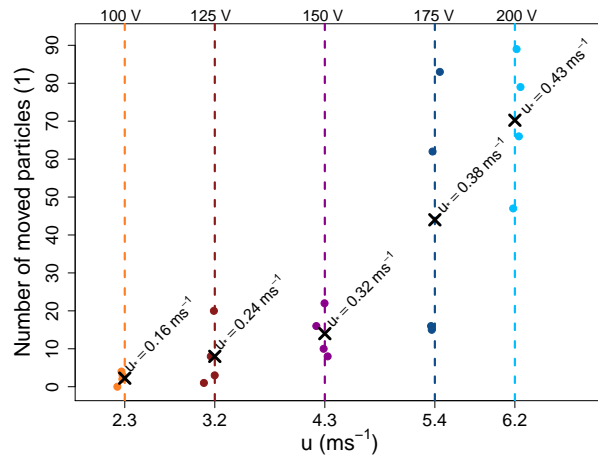
With rising wind speed, the number of particles that moved is also rising, from two to 70 particles (Fig. 4.7a). The range of wind speed throughout the different experiment lengths is relatively small. The difference between positive and negative particles, which indicates how many particles were actually blown off the glass slide (Fig. 4.7b), shows that higher wind speeds lead to larger differences and therefore that more particles were blown away. This finding confirms the origin expectation that there is a difference in particle movement due to different wind speeds.

It was a decrease in the rate of particle movement after the first minutes expected because in this time range most of the particles that can be moved easily should be detached from the glass slide by the erosivity of the wind. After that, the erosivity should not be large enough to move the other particles which can only be moved by eddies with more energy (Fig. 2.3). Therefore, the rate of erosion should decrease with longer experiment lengths.

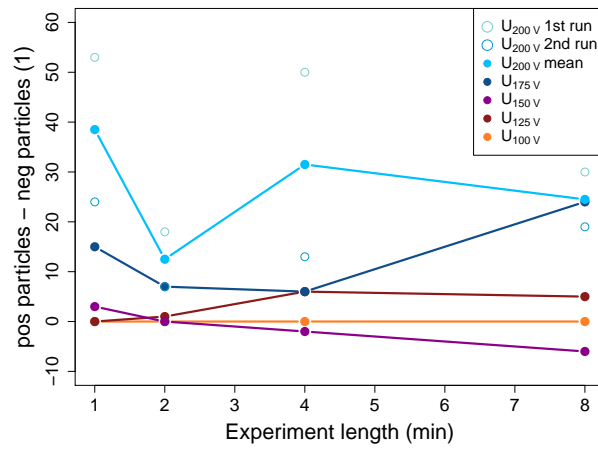
Figure 4.8 should be, theoretically, a cumulative plot as the number of moved particles (positive particles) in the experiment with one minute experiment length should also be contained in the number of moved particles for the experiment with a length of two minutes. This is only theoretical because each experiment was conducted with another glass slide. At low wind speeds, the number of moved particles does not increase noticeably with longer experiment lengths. At a wind speed of  $2.3 \text{ ms}^{-1}$  (fan setting of 100 V), there are at most 4 particles moving. At a wind speed of  $3.2 \text{ ms}^{-1}$  (fan setting of 125 V), the peak in particle movement is at 4 minutes experiment length with 20 particles. This number gets reduced by more than a half to 8 particles at an experiment length of 8 minutes. This number is still higher than at 1 or 2 minutes (1 and 3 particles). At a wind speed of  $4.3 \text{ ms}^{-1}$  (fan setting of 150 Volt), the peak is at 2 minutes with 22 particles, after that, there are only 10 and 16 particles moving at 4 and 8 minutes experiment length but these numbers are still in the same range.

The irregularities seen in experiment experiment block B in Table 4.2 for higher wind speeds are now shown in Figure 4.8a. At  $5.4 \text{ ms}^{-1}$  (175 Volt), the value for 1 minute experiment length is extremely high with 83, even higher than at the wind speed for the wind tunnel setting of 200 Volt. At 2 and 4 minutes however, less than a quarter of the particles are moving (15 and 16) and then, the number rises up again to 62 at 8 minutes. At the highest wind speed (fan setting of 200 V), the trend is different than at the wind speeds. At four minutes, the most particles moved with a number of 89. However, at 8 minutes, it's the lowest value of this voltage stage with 47 particles.

Methodical decisions could explain these discrepancies. Every data point

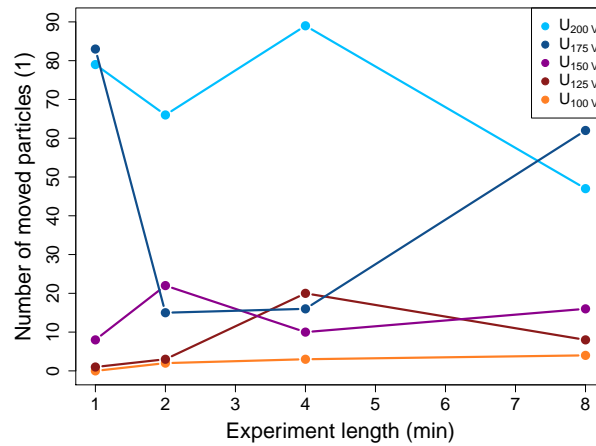


(a) Particle movement over wind speed. The dashed lines show the mean wind speed per fan speed setting. The crosses indicate the mean number of moved particles over the four different experiment lengths per fan speed setting. The friction velocity was calculated earlier (Fig. 3.7).

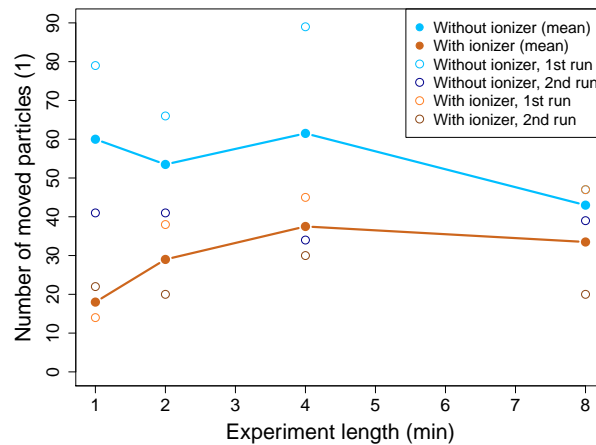


(b) Difference between positive and negative particle values over experiment length of experiments 13 to 36 at five different fan speed settings. First run describes experiments 29 to 32, second run means experiments 33 to 36.

**Figure 4.7:** Comparison of particle movement related to wind speed at five different wind speeds (experiments 13 to 36). No ionizer was used for these experiments.



(a) Number of moved particles of experiments 13 to 32 at different wind speeds ( $2.3 \text{ ms}^{-1}$ ,  $3.2 \text{ ms}^{-1}$ ,  $4.3 \text{ ms}^{-1}$ ,  $5.4 \text{ ms}^{-1}$  and  $6.2 \text{ ms}^{-1}$ )



(b) Number of moved particles of experiments 29 to 36 (without ionizer, blue dots) and 37 to 44 (with ionizer, orange dots) at a wind speed of  $6.3 \text{ ms}^{-1}$

**Figure 4.8:** Comparison of particle movement over experiment length related to wind speed of five different wind tunnel configurations (a) and variation in ionization (b) (Table 4.2)

was measured with an individual glass slide. Thus, not only the distribution on the glass slide was different for every experiment but also the electric charge of the particles and the glass slide, and therefore the adhesion forces, could vary. These differences at experiments 25 to 28 and experiments 29 to 32 might be explained by that. Another explanation could be that the ionization in the

wind tunnel varied throughout the experiments, as they were done over several hours. As a third idea, the turbulent flow in the tunnel may be not constant. The hot wire anemometer did not record noticeable differences in turbulence intensity but its accuracy in velocity is 0.1 to 0.2  $\text{ms}^{-1}$  at 5 to 10  $\text{ms}^{-1}$  wind speed. As the turbulence intensity is calculated by the division of standard deviation and mean of the wind speed, smaller eddies cannot be measured.

The mean of the experiments 29 to 32 and 33 to 36 is flatter compared to the zig zag line of the experiment block B (light blue line Fig. 4.8b compared to a) so that the difference between the particle movement of 1 minute and 8 minutes experiment length (experiments 29 and 32) gets smaller. The number of particles that are moving in the second run without ionizer (experiments 33 to 36) are all in the same range (dark blue dots, Fig. 4.8). One minute and two minutes experiment length show no difference in particle movement for the second run. At four minutes, it is a bit less with 34 particles instead of 41 but at eight minutes, 39 particles are moving. Looking at the mean line of the experiments with ionizer (light brown line in Fig. 4.8b), only five particles more are moving at four minutes than at eight. Here, the line is almost as expected, the decrease in the rate of erosion is well recognizable.

Overall, due to only a few data points, it is difficult to see the expected trend. It can be observed the best with ionizer at the highest wind speed of 6.3  $\text{ms}^{-1}$  (fan setting of 200 V).

The critical friction velocity was found using experiment block B. The mean number of moved particles over all four experiment lengths at wind speeds 2.3 and 3.2  $\text{ms}^{-1}$  is below ten (Fig. 4.7a). At a mean wind speed of 3.2  $\text{ms}^{-1}$ , the mean over all experiment lengths is only eight particles that are moving. The highest difference of positive and negative particles, that is the number of particles that were actually blown away from the glass slide, was at four and eight minutes experiment length. At these experiment lengths, six and five particles actually left the glass slide (Fig. 4.7b). At a mean wind speed of 2.3  $\text{ms}^{-1}$  (fan setting of 100 V), only 2.25 particles moved in average over all experiment lengths (mean of number of positive particles of experiments 13 to 16, Table 4.2) but no particle left the glass slide as the difference of positive and negative particles is zero for each experiment length. In fact, the particles only moved distances on the order of micrometers and stayed on the glass slide.

As 11 particles were blown away at a wind speed of 3.2  $\text{ms}^{-1}$  but none at a wind speed of 2.3  $\text{ms}^{-1}$ , these wind speeds form the range for the corresponding critical friction velocity:  $u_*$  lies in between 0.16  $\text{ms}^{-1}$  and 0.24  $\text{ms}^{-1}$  for the conditions at that day (Fig. 3.7a,b). Compared to the findings of Shao et al. (2000) for sand particles, this is a lower value than for a sand sphere of the

same diameter ( $0.2 - 0.3 \text{ ms}^{-1}$ ). One of the main influencing factors for this could be the density which is much lower for the polyethylene spheres that were used here than for a quartz corn ( $1.00 \text{ gcm}^{-3}$  compared to  $2.65 \text{ gcm}^{-3}$ ). Comparing the results with other studies on MP is difficult as there are only two known studies examining microplastic spheres in a wind tunnel (Wu et al., 1992; Kim et al., 2016) but they are focusing on resuspension rates and not on threshold friction velocities.

### 4.2.2 Impact of interparticle forces on MP suspension

In experiment block A, the ionizer was turned on and off irregularly but the results demonstrate its influence (Table 4.2). Comparing experiment 10 and experiment 30, for example, the number of positive particles from the experiment with the ionizer differed by up to a factor of 5 from the experiments taken without ionizer (310 particles to 66 particles). Due to this huge decrease in particle movement without ionizer, some more systematical experiments were done at a high wind speed of  $6.3 \text{ ms}^{-1}$  as the relative error gets smaller the more particles are moving. Experiments 29 to 36 were conducted without ionizer, 37 to 44 with ionizer.

The effects of the ionizer from experiment block A with a factor of 5 cannot be seen in the results of experiment block C (Table 4.2). In fact, the results of the experiments 37 to 44 even show a lower number of moved particles than 29 to 36 (Fig. 4.8). The mean of the positive particle movement over all experiment lengths without the ionizer was 56.75 particles whereas the mean with ionizer was only 31.25.

Looking at the comparison of using and not using an ionizer during the experiments, the results did not show what was expected. It was assumed that using an ionizer would balance the difference in electrical charge between the glass slide and the particles and would also equalize the ionization in the tunnel. More particles should be blown away as the difference in electrical charge should be smaller. However, the results suggest that there are more forces to consider than first thought.

As Wu et al. (1992) underlines in their research, relative humidity plays an important role in resuspension rates. Hence, the humidity values for the Ecological Botanical Garden in Bayreuth, near the laboratory, were used in Figure 4.9.

Experiments 29 to 32 were done on October 19th in the evening whereas experiments 33 to 36 were conducted on October 25th in the morning. The experiments with ionizer were done on October 25th in the evening. The relative humidity was calculated by using the absolute humidity values from the Botanical Garden and relate them to the temperature in the laboratory,

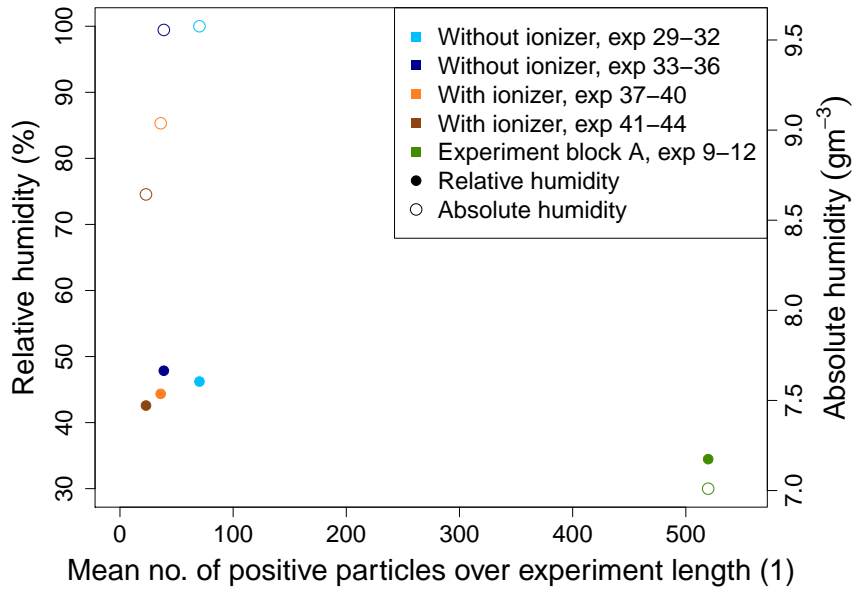


**Figure 4.9:** Comparison of number of moved particles of experiments 29 to 32 (1st run without ionizer), 33 to 36 (2nd run without ionizer), 37 to 40 (1st run with ionizer), 41 to 44 (2nd run with ionizer) and 9 to 12 (experiment block A) at a wind speed of  $6.3 \text{ ms}^{-1}$  with corresponding humidity values in the laboratory

which was also measured by the hot wire anemometer. It was between  $22.5$  and  $23.2 \text{ }^\circ\text{C}$ .

The relative humidity values for the experiments of B and C (filled dots) are between  $40$  and  $50 \%$  whereas the absolute humidity (unfilled circles) is between  $8.5$  and  $9.6 \text{ gm}^{-3}$  (Fig. 4.9). The absolute humidity at the time of experiments 9 to 12 was lower with  $7.0 \text{ gm}^{-3}$ , hence also the relative humidity is lower with  $34 \%$ .

Corn (1961) summarized the link between adhesion force and humidity and concluded that relative humidity has a great effect on the adhesion forces but due to different theories, the nature of the influence was not clear.

Ranade (1987) examined in his research the adhesion forces of small particles on surfaces. He also took condensation between bodies in account which causes an attractive force and underlined that condensation of water vapour can begin at a relative humidity of  $65$  to  $70 \%$ . This can be explained by the Kelvin equation which states that the vapour pressure over convex surfaces is higher than over flat surfaces. Due to negative curvature in the particle-surface-interface, condensation can also occur despite undersaturated air.

Even though there was more particle movement at experiment block A,

the relative humidity was only slightly below the values of the days of experiment blocks B and C. However, the relative humidities of all experiments are below the condensation values in the literature. Hence, condensation may not yet be significant here. The expectation that the suspension rate of MP particles is lower at higher relative humidities cannot be confirmed with this data. However, the validity of this plot has to be increased in further studies by measuring humidity values in the laboratory.

Kim et al. (2016) studied resuspension rates by aerodynamic forces of glass and polyethylene particles on three different surfaces, glass slides amongst them. They used particles of approximately 19  $\mu\text{m}$  and 37  $\mu\text{m}$  and found that a relative humidity higher than 60 % reduced the resuspension rate of the smaller particles significantly. However, the impact on the larger particles was smaller because with increasing size, the ratio of the total area that is in contact with the surface, decreases. Therefore, effects on the particle concerning particle-surface interactions are relatively less important.

Even though the particle size was bigger than in the study of Kim and relative humidities above 60 % were not reached, the study showed that the impact of relative humidity was bigger on hydrophilic surfaces as glass than on hydrophobic surfaces like gold for hydrophobic particles (Kim et al., 2016). As glass slides were used in this study, it underlines the importance of humidity measurements during the experiments.

## 5. Conclusion

One of the objectives of this research was to test different detection methods for fluorescent MP particles in a wind tunnel and to compare them in order to find a practicable and precise method. As the chemical approach with the fluorometer led to very unstable and imprecise results and the fluorescence microscopy was very time consuming and created huge data files, the photometric method performed the best in this research. Setting the construction up and taking a picture of the sample only takes a couple of minutes. With a little adjustment of the construction, the evaluation could be even more simplified. This method is very precise as the movement of every particle is visible. Another point is that it is transportable so that it can be easily installed right next to the wind tunnel to reduce the error of the sample as much as possible.

The experiments in the wind tunnel proofed the applicability of the photometric method and delivered some knowledge about MP suspension. As expected, there was more particle movement with higher wind speed. However, the movement over the varying experiment length showed some inconsistencies. This finding could be due to the fact that for every experiment another sample was used, so the electrical charge of the particles and the slide could have varied. This methodological decision should be changed in further wind tunnel studies. The critical friction velocity could be set to a range between  $0.16 \text{ ms}^{-1}$  and  $0.24 \text{ ms}^{-1}$  for the conditions in the laboratory. The experiments with and without ionizer indicated that there are more factors to be considered than just electrical force as the results differed from the expectation. More studies are needed to systematically characterize the impact factors on MP suspension. Measuring the relative humidity in the laboratory should be included in further studies as it might be an important factor on the suspension.

Starting with spheres as the best understood form, more parameter such as shape and size of the particles can be varied in further experiments as well as the surface of the testing area to successively reach environmental conditions. The study showed that various factors beside particle properties influence the suspension of MP particles, such as wind speed, critical friction velocity, electrical force and humidity. The photometric method is a precise and fast detection method for MP particles in further wind tunnel studies.



# Acknowledgement

I would like to thank the whole Micrometeorology Group for supporting me and helping me whenever I needed it.

A special thanks goes to my supervisor Prof. Dr. Christoph Thomas who started this journey of blowing fluorescent particles in the wind tunnel and made this work possible. I also thank Prof. Dr. Martin Obst for the second revision, the introduction to the fluorescent microscope and for the idea of an optical construction as an alternative to the microscope. A big thanks goes to Dr. Karl Lapo, Lena Pfister and Anita Freundorfer for introducing me to the laboratory work and for always helping me out. I also thank Johann Schneider for the constant help in the laboratory. Thanks to Dr. Wolfgang Babel for the support and help with R.

Thanks also to Dr. Ben Gilfedder, Silke Hammer and Jutta Eckert for helping me with the fluorometer and supporting me with ideas and supplies.

# Appendix

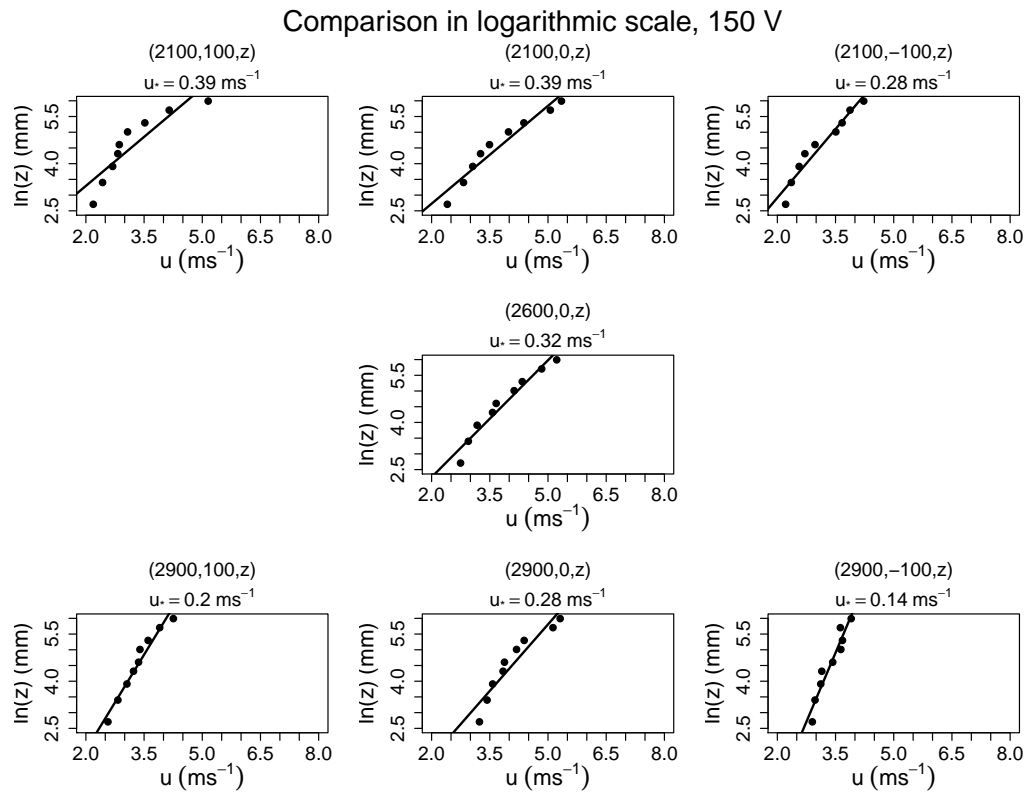


Figure 6.1: Logarithmic wind profiles at different locations in the adjusted wind tunnel at a wind tunnel setting of 150 V (unit of locations: mm). The plots are arranged from the top view of the tunnel.

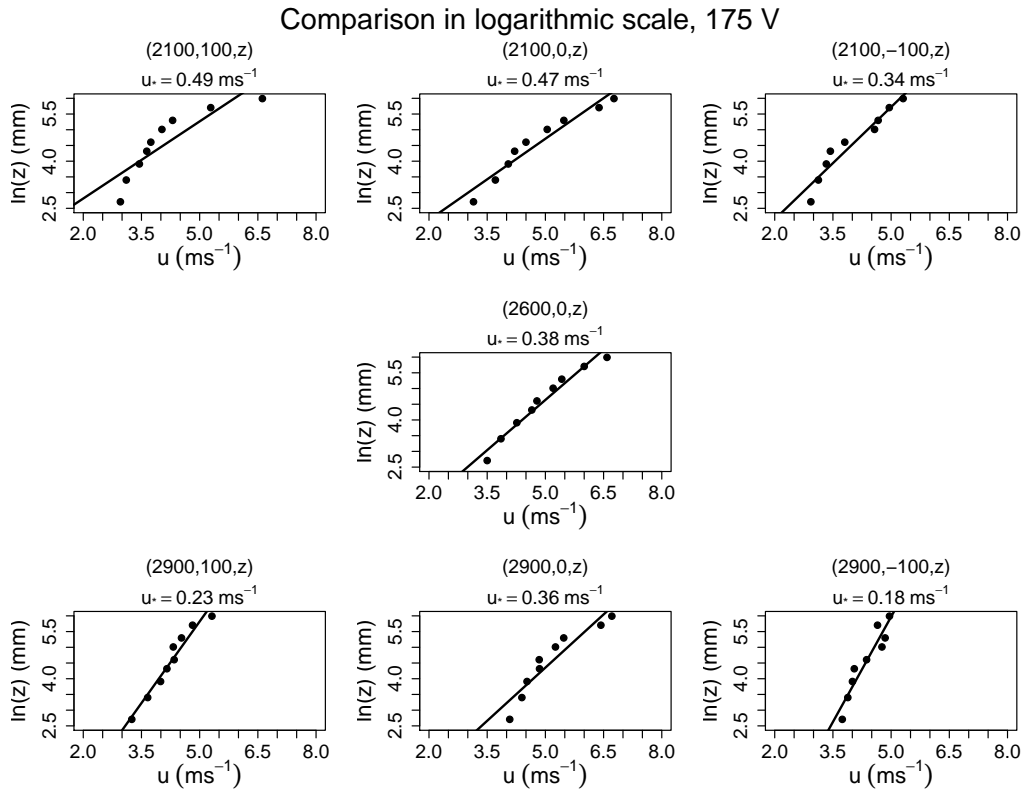


Figure 6.2: Logarithmic wind profiles at different locations in the adjusted wind tunnel at a wind tunnel setting of 175 V (unit of locations: mm). The plots are arranged from the top view of the tunnel.

# Bibliography

- Alencastro, D (2012). “Pollution due to plastics and microplastics in Lake Geneva and in the Mediterranean Sea”. In: *Archives des Sciences* 65, pp. 157–164.
- Bagnold, R. A. (1973). *The physics of blown sand and desert dunes*. Chapman and Hall, Methuen, London.
- Barnes, David KA et al. (2009). “Accumulation and fragmentation of plastic debris in global environments”. In: *Philosophical Transactions of the Royal Society of London B: Biological Sciences* 364.1526, pp. 1985–1998.
- Beladjine, Djaoued et al. (2007). “Collision process between an incident bead and a three-dimensional granular packing”. In: *Physical Review E* 75.6, p. 061305.
- Chepil, WS (1956). “Influence of Moisture on Erodibility of Soil by Wind 1”. In: *Soil Science Society of America Journal* 20.2, pp. 288–292.
- Cole, Matthew et al. (2011). “Microplastics as contaminants in the marine environment: a review”. In: *Marine pollution bulletin* 62.12, pp. 2588–2597.
- Cook, Paul F and William Wallace Cleland (2007). *Enzyme kinetics and mechanism*. Garland Science.
- Corn, Morton (1961). “The adhesion of solid particles to solid surfaces, I. A review”. In: *Journal of the Air Pollution Control Association* 11.11, pp. 523–528.
- Dris, Rachid (2016). “First assessment of sources and fate of macro-and microplastics in urban hydrosystems: Case of Paris megacity”. PhD thesis. UPE, Université Paris-Est.
- Dris, Rachid et al. (2015). “Beyond the ocean: contamination of freshwater ecosystems with (micro-) plastic particles”. In: *Environmental Chemistry* 12.5, pp. 539–550.
- Dris, Rachid et al. (2016). “Synthetic fibers in atmospheric fallout: a source of microplastics in the environment?” In: *Marine pollution bulletin* 104.1-2, pp. 290–293.
- Fletcher, B (1976a). “The erosion of dust by an airflow”. In: *Journal of Physics D: Applied Physics* 9.6, p. 913.
- (1976b). “The incipient motion of granular materials”. In: *Journal of Physics D: Applied Physics* 9.17, p. 2471.

- Greeley, R and JD Iversen (1985). “Wind as a geological process, no. 4 in Cambridge Planetary Science Series”. In: *Cambridge Univ. Press, New York, NY* 3.3, pp. 3–2.
- Gromke, C and B Ruck (2005). “Die Simulation atmosphärischer Grenzschichten in Windkanälen”. In: *Proc. 13. GALA Fachtagung” Lasermethoden in der Strömungsmesstechnik*, pp. 51–1.
- Ho, T (2012). “Experimental study of saltating particles in a turbulent boundary layer”. PhD thesis. University of Rennes 1.
- Ho, Tuan Duc et al. (2011). “Scaling laws in aeolian sand transport”. In: *Physical Review Letters* 106.9, p. 094501.
- Huerta Lwanga, Esperanza et al. (2016). “Microplastics in the terrestrial ecosystem: implications for *Lumbricus terrestris* (Oligochaeta, Lumbricidae)”. In: *Environmental science & technology* 50.5, pp. 2685–2691.
- Imhof, Hannes K et al. (2013). “Contamination of beach sediments of a sub-alpine lake with microplastic particles”. In: *Current biology* 23.19, R867–R868.
- Jambeck, Jenna R et al. (2015). “Plastic waste inputs from land into the ocean”. In: *Science* 347.6223, pp. 768–771. URL: [https://wedocs.unep.org/bitstream/handle/20.500.11822/17969/Plastic\\_waste\\_inputs\\_from\\_land\\_into\\_the\\_ocean.pdf?sequence=1](https://wedocs.unep.org/bitstream/handle/20.500.11822/17969/Plastic_waste_inputs_from_land_into_the_ocean.pdf?sequence=1).
- Kim, Yoojeong et al. (2016). “Effects of relative humidity and particle and surface properties on particle resuspension rates”. In: *Aerosol Science and Technology* 50.4, pp. 339–352.
- Klein, Sascha, Eckhard Worch, and Thomas P Knepper (2015). “Occurrence and spatial distribution of microplastics in river shore sediments of the Rhine-Main area in Germany”. In: *Environmental science & technology* 49.10, pp. 6070–6076.
- Lakowicz, Joseph R. (2006). *Principles of Fluorescence Spectroscopy*. Springer Science+Business Media. ISBN: 0-387-31278-1.
- Lambert, Scott, Chris Sinclair, and Alistair Boxall (2014). “Occurrence, degradation, and effect of polymer-based materials in the environment”. In: *Reviews of Environmental Contamination and Toxicology, Volume 227*. Springer, pp. 1–53.
- Liebmann, Bettina et al. (2018). *Assessment of microplastic concentrations in human stool - Preliminary results of a prospective study*. URL: [http://www.umweltbundesamt.at/fileadmin/site/presse/news\\_2018/UEG\\_Week\\_2018\\_-\\_Philipp\\_Schwabl\\_Microplastics\\_Web.pdf](http://www.umweltbundesamt.at/fileadmin/site/presse/news_2018/UEG_Week_2018_-_Philipp_Schwabl_Microplastics_Web.pdf).
- McKenna-Neuman, C and WG Nickling (1989). “A theoretical and wind tunnel investigation of the effect of capillary water on the entrainment of sediment by wind”. In: *Canadian Journal of Soil Science* 69.1, pp. 79–96.

- Nizzetto, Luca, Martyn Futter, and Sindre Langaas (2016). *Are agricultural soils dumps for microplastics of urban origin?*
- Parker, ST and RP Kinnersley (2004). “A computational and wind tunnel study of particle dry deposition in complex topography”. In: *Atmospheric Environment* 38.23, pp. 3867–3878.
- Peeken, Ilka et al. (2018). “Arctic sea ice is an important temporal sink and means of transport for microplastic”. In: *Nature communications* 9.1, p. 1505.
- PlasticsEurope (2018). *Plastic - the facts 2017: An analysis of European plastics production, demand and waste data*. URL: [https://www.plasticseurope.org/application/files/5715/1717/4180/Plastics\\_the\\_facts\\_2017\\_FINAL\\_for\\_website\\_one\\_page.pdf](https://www.plasticseurope.org/application/files/5715/1717/4180/Plastics_the_facts_2017_FINAL_for_website_one_page.pdf).
- Prandtl, Ludwig (1934). “The Mechanics of Viscous Fluids”. In: *Aerodynamic Theory* 3. Ed. by W. F. Durand, pp. 33–207.
- Ranade, MB (1987). “Adhesion and removal of fine particles on surfaces”. In: *Aerosol Science and Technology* 7.2, pp. 161–176.
- Rice, MA, IK McEwan, and CE Mullins (1999). “A conceptual model of wind erosion of soil surfaces by saltating particles”. In: *Earth Surface Processes and Landforms: The Journal of the British Geomorphological Research Group* 24.5, pp. 383–392.
- Rice, MA and IK McEwan (2001). “Crust strength: a wind tunnel study of the effect of impact by saltating particles on cohesive soil surfaces”. In: *Earth Surface Processes and Landforms: The Journal of the British Geomorphological Research Group* 26.7, pp. 721–733.
- Rillig, Matthias C. (2012). “Microplastic in Terrestrial Ecosystems and the Soil?” In: *Environmental Science & Technology* 46.12. PMID: 22676039, pp. 6453–6454. DOI: 10.1021/es302011r. URL: <https://doi.org/10.1021/es302011r>.
- Shao, Yaping (2000). *Physics and Modelling of Wind Erosion*. Atmospheric and Oceanographic sciences library. Kluwer Academic Publishers. ISBN: 0-7923-6657-3.
- Shao, Yaping and Hua Lu (2000). “A simple expression for wind erosion threshold friction velocity”. In: *Journal of Geophysical Research: Atmospheres* 105.D17, pp. 22437–22443.
- Shao, Yaping and An Li (1999). “Numerical modelling of saltation in the atmospheric surface layer”. In: *Boundary-Layer Meteorology* 91.2, pp. 199–225.
- Shao, YP, Michael R Raupach, and John F Leys (1996). “A model for predicting aeolian sand drift and dust entrainment on scales from paddock to region”. In: *Soil Research* 34.3, pp. 309–342.

- Shojaee, SMN, O Uzol, and Ö Kurç (2014). “Atmospheric boundary layer simulation in a short wind tunnel”. In: *International Journal of Environmental Science and Technology* 11.1, pp. 59–68.
- Souza Machado, Anderson Abel de et al. (2018). “Microplastics as an emerging threat to terrestrial ecosystems”. In: *Global change biology* 24.4, pp. 1405–1416.
- Wu, Yee-Lin, Cliff I Davidson, and Armistead G Russell (1992). “Controlled wind tunnel experiments for particle bounceoff and resuspension”. In: *Aerosol Science and Technology* 17.4, pp. 245–262.
- Zubris, Kimberly Ann V and Brian K Richards (2005). “Synthetic fibers as an indicator of land application of sludge”. In: *Environmental pollution* 138.2, pp. 201–211.



# Declaration of Authorship

I declare that I completed this thesis on my own and that information which has been directly or indirectly taken from other sources has been noted as such. Neither this nor a similar work has been presented to an examination committee.

Bayreuth, March 6, 2019

.....